[M{κ^2*S,S*-S_2C-piperazine-C_2H_4N=C(R)}$_n$] {Co(III), Ni(II), Cu(II) or Zn(II)} complexes bearing pendant Schiff base moieties: Spectral characterization, fluorescence, cyclic voltammetric and TGA/DTA study

Abstract

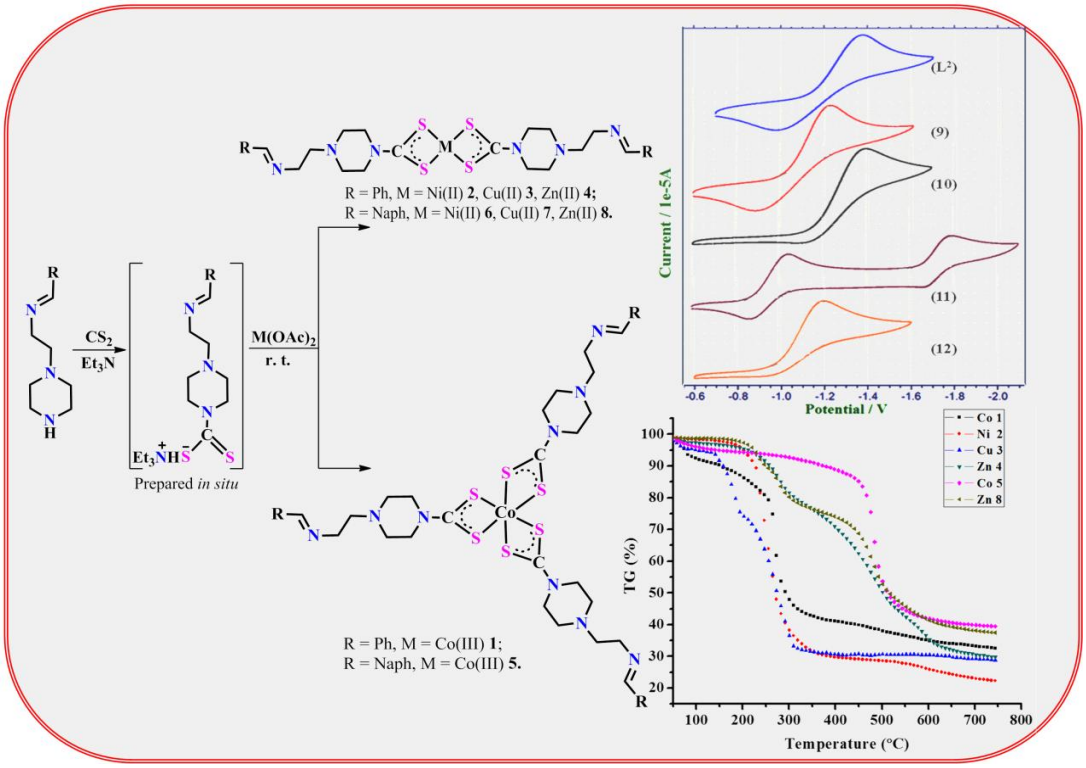

A series of neutral mononuclear complexes [M{κ^2*S,S*-S_2C-piperazine-C_2H_4N=C(R)}$_n$]{R = Ph; M = Co(III) **1**, Ni(II) **2**, Cu(II) **3**, Zn(II) **4**; R = Naph; M = Co(III) **5**, Ni(II) **6**, Cu(II) **7**, Zn(II) **8**; n = 2 for **2-4**, **6-8** and n = 3 for **1**, **5**} bearing pendant Schiff base moieties were efficiently synthesized through self-assembly process involving the novel amine precursor N-[phenylmethylidene]-2-piperazin-1-ylethanamine (L^1) or N-[naphthylmethylidene]-2-piperazin-1-ylethanamine (L^2) with two equivalents each of CS_2 and corresponding metal acetates. All the mononuclear complexes **1-8** were characterized by microanalysis and relevant spectroscopic methods such as ESI MS, IR, ^{1}H, ^{13}C NMR, DEPT 135, UV-visible absorption and emission spectroscopy. Complexes **1**, **3** and **8** exhibit maximum fluorescence emissions at 342, 344 and 348 nm upon excitation at 273 (for complex **1** and **3**) and 263 (for complex **8**) with concomitant Stokes shifts of ≈ 69 nm, ≈ 71 nm and ≈ 85 nm. The spectral and magnetic moment data supports octahedral geometry around

Co(III) and square planar/ tetrahedral geometry around other metal centres. Thermal stability of complexes **1-8** has been investigated by thermogravimteric analysis. The cyclic voltammograms clearly suggest that the mononuclear complexes exhibit electroreduction principally associated with pendant imine moieties except Cu(II) complex **7** which display quasi-reversible reduction corresponds to the Cu(II)/Cu(I) redox couples, in addition to the reversible electroreduction of pendant imine groups associated with the coordinated ligands.

3B.1. Introduction

Transition metal complexes derived from sulphur rich ligands a exhibit wide range of applications in the area of electrical conductivity, molecular magnetism, electrochemical, biological processes and optoelectronic properties [1]. Among these ligands, the dithiocarbamates have been emerged as a versatile and of particular interest due to the ease of synthesis and their ability to bind to all the transition elements supporting a wide range of oxidation states [2]. They find their potential uses in the medicine due to the existence of dithiocarbamate moiety in a variety of biologically active molecules [3]. Many dithiocarbamate complexes have been used as a single source precursor for the synthesis of high-quality semi-conductor nanoparticles [4]. Thermogravimetric study of dithiocarbamate complexes advocate their wide spread industrial applications such as foam rubber, fungicides, effective heat stabilizers, antioxidant action, reprocessing of polymers [5]. It further suggests the suitability of complexes to be used as single source precursors for the synthesis of metal sulphide nano particles and thin films [6]. The size and shape of the metal sulphide nanoparticles greatly depend on the nature of organic moiety present in metal dithiocarbamate complexes which sequentially affect the fundamental properties such as optical, electrical and mechanical [7].

While enormous number of dithiocarbamate complexes containing simple alkyl/aryl substituents have been synthesized and their study is well documented in literature, however, functionalization of the backbone of these dithiocarbamate ligands is still in its early stage [8]. It offers new dimensions of applications and interactions *viz* functionalization of gold nanoparticles [9], the synthesis of supramolecular systems which can be used for anion binding [10], the development of

radiopharmaceuticals [11] and efficient chelators for the treatment of acute cadmium intoxication [12].

Recently a number of reports have been emerged on the potential applicability of piperazine derivatives. For instance, piperazinyl linked ciprofloxacine dimers and other derivatives of piperazine are appeared as potent antibacterial agents against resistant strains, dual calcium antagonist, antimalarial agents, antifungal agents and potential antipsychotic agents [13]. However dithiocarbamate derivatives of functionalized piperazine and their transition metal complexes are far less studied [2d].

Thus, in the light of these observations, we undertake the synthesis of simple functionalized dithiocarbamate complexes based on N-[arylmethylidene]-2-piperazin-1-ylethanamine backbones bearing pendant Schiff base moieties. These complexes are thoroughly characterized by microanalysis, ESI MS, FT-IR, ^{1}H and ^{13}C NMR, UV-visible absorption, fluorescence, thermogravimetric and cyclic voltammetric studies.

3B.2. Result and Discussion

3B.2.1. Synthesis and characterization

Condensation of 1-(2-aminoethyl)-piperazine with benzaldehyde or naphthaldehyde in toluene in acidic medium yielded the corresponding amine derivatives N-[phenylmethylidene]-2-piperazin-1-ylethanamine (L^1) and N-[naphthylmethylidene]-2-piperazin-1-ylethanamine (L^2) in good yields (Scheme 1). The self-assembly process involving these novel amines L^1or L^2 with two equivalents each of CS_2 and corresponding metal acetates affords access to a new series of functionalized mononuclear dithiocarbamate complexes [M{κ^2*S*,*S*-S_2C-piperazine-C_2H_4N=C(R)}$_n$]{R = Ph; M = Co(III) **1**, Ni(II) **2**, Cu(II) **3**, Zn(II) **4**; R = Naph; M = Co(III) **5**, Ni(II) **6**, Cu(II) **7**, Zn(II) **8**; n = 2 for **2-4**, **6-8** and n = 3 for **1**, **5**} bearing pendant Schiff base moieties (Scheme 2). These complexes show moderate

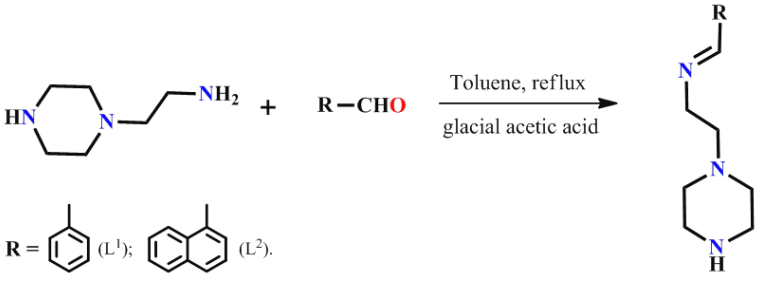

Scheme 1. Preparation of ligand precursors L^1 and L^2.

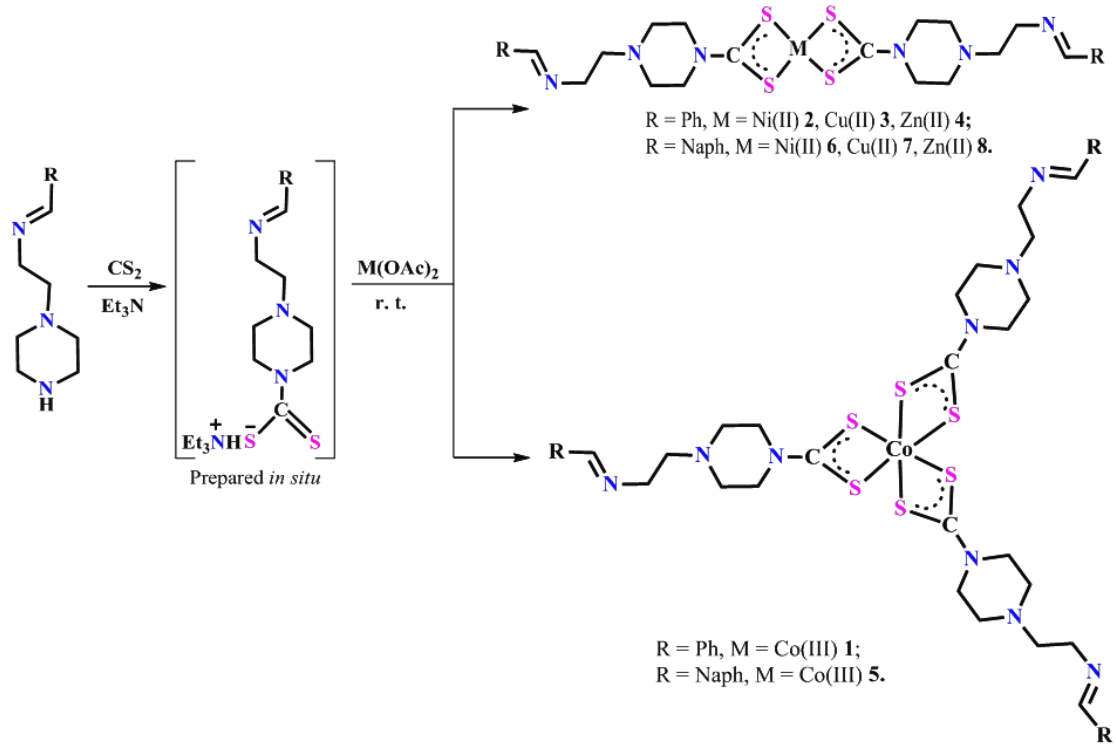

Scheme 2. Preparation of mononuclear dithiocarbamate complexes **1-8**.

to poor solubility in common organic solvents and found to be stable in solid state and in the solution over a period of days. The poor solubility of the majority of these complexes most likely relates to the large number of intermolecular interactions. Our attempts to grow single crystals suitable for single crystal X-ray diffraction study were unsuccessful. Similar complexes of heavy metals were previously derived [14] from piperazine derivatives such as *N*-[*β*-2,5-dimethyl-1-pyrrolyl)ethyl]piperazine and N-[*β*-salicylideneaminoethyl)]piperazine bearing protected amino-groups. It has been experienced by Professor Hogarth and his co-workers that bis(dithiocarbamate) complexes with functionalised backbones can easily be prepared but their crystallization can be more problematic. [15] The precursors L^1, L^2 and mononuclear complexes were characterized by microanalysis and standard spectroscopy. The ESI-MS of the complexes **4** and **6** gave molecular ion peaks at m/z 651.1 and 745.0 respectively, which corresponds to $[M+H]^+$ along with differential fragmentation peaks (supplementary information).

3B.2.2. IR spectral study

The characteristic IR bands for L^1, L^2 and mononuclear bis- dithiocarbamato complexes **1-8** are summarized in the experimental section. A comparison of IR spectra of the complexes with the precursors L^1, L^2 indicates that the υ(N-H) band (3200-3300 cm^{-1}) seen for L^1 and L^2 (supporting information) is disappeared from the IR spectra of all the complexes **1-8** and two new single sharp medium intensity bands are appeared in the regions of 1474-1509 cm^{-1} and 994-1003 cm^{-1}, confirms the coordination of dithiocarbamate lignads in a bidentate fashion. [16] These two regions are associated with ν(N-CS_2) and ν(S-C) stretching frequencies, respectively and these are of particular interest in the IR spectral study of dithiocarbamates complexes. The values of ν(N-CS_2) stretchings (1474-1509 cm^{-1}) are between the range reported for C=N double bond (1650-1690 cm^{-1}) and C-N single bond (1250-1350 cm^{-1}), indicative of partial double bond character of N-CS_2 bonds, which would result in some partial double bond character for the C–S bonds..This is due to the mesomeric drift of an electron cloud of the dithiocarbamate (–NCS_2) moiety towards the metal ion and confirmed an increase in the C–N double bond character. In addition to these new bands, all complexes exhibit bands in the range of 3047-2932, 1649-1639 and 1509-1456 cm^{-1} due to υ(C–H), υ(C=N) and υ(C=C) stretching frequencies respectively, which are associated with aromatic stretching frequency of phenyl/ naphthyl and imine moiety of the ligand fragment in **1-8**. Interestingly, there is no significant change in the υ(C=N) band observed for the complexes, compared to their precursors L^1 (1644 cm^{-1}) and L^2 (1649 cm^{-1}) which give strong evidence for the presence of pendant Schiff base moieties in these complexes. In conclusion the dithiocarbamato ligands generated *in situ* from L^1 and L^2 behaves as a monobasic bidentate in all the complexes **1-8**.

3B.2.3. NMR spectral study

The ^1H NMR spectra of precursors L^1, L^2 display most characteristic signals at δ 2.29, 3.15 ppm and 8.33, 9.07 ppm which are attributable to amine (–NH) and imine protons, whereas signals appeared in the range of 2.38−3.69 ppm and 7.15-7.73 ppm are associated with the aliphatic methylene and aromatic protons, respectively. The disappearance of amine signals and noticeable downfield shifting of aliphatic/aromatic NMR signals of complexes **2**, **4** and **8**, compared to L^1 and L^2 (supporting information) confirms the involvement of these precursors in

dithiocarbamate complex formation. The ^{13}C NMR spectra of the complexes **2** and **4** display a very downfield signal at 210.6 and 193.6 ppm, characteristic of coordinated dithiocarbamate (-N*C*S_2) ligands. [17] In addition to the aliphatic and aromatic ^{13}C signals, these complexes further display signals at 194.6 and 161.5 ppm due to imine '-H*C*=N-' carbons. Notably, a significant downfield shifting of the NMR signals (especially imine '-CH=N)' group and dithiocarbamate '–NCS_2' group signals) of **2** was observed, when compared to the similar signals of **4** and **8** whose spectra were taken in normal DMSO-*d6*. The assignments of ^{13}C signals of $\mathbf{L^1}$, $\mathbf{L^2}$ and complex **2** are supported by DEPT 135 NMR spectral study which clearly distinguished the imine and aromatic carbons (appears in the positive region) from aliphatic methylene carbons (appears in negative region). Interestingly, no significant shifting of imine (-C*H*=N) proton signals were observed in the complexes **4** and **8**, compared to their positions in the precursors L^1 and L^2 and this rule out the possibility of involvement of Schiff base moieties in coordination.

3B.2.4. UV-visible absorption and magnetic moment study

The UV–visible absorption properties of ligand precursors $\mathbf{L^1}$ and $\mathbf{L^2}$ and mononuclear dithiocarbamate complexes **1-8** were investigated at room temperature from 10^{-5} M DMSO solution samples and the pertinent results are summarized in Table 1. The assignment of UV-visible absorption bands are based on the literature reports on closely related compounds. [18] The UV-visible absorption spectra of the precursors and mononuclear complexes are shown in Figure 1 and 2. Principally, both the precursors $\mathbf{L^1}$ and $\mathbf{L^2}$ exhibit a single prominent band at shorter wavelength 260 and 288 nm respectively, assigned to $\pi \rightarrow \pi^*$ (phenyl) transitions [19]. All the dithiocarbamato complexes **1-8** exhibit maximum absorbance at 273, 259, 273, 263, 273, 259, 274 and 263 nm with the molar extinction coefficient values of 54975, 52283, 44235, 66853, 55376, 47803, 75967 and 53597 respectively associated with the dithiocarbamate ligand moiety are assigned to the N–C=S group. The bands at 325, 388, 439, 326, 388 and 437 nm observed for the mononuclear dithiocarbamato complexes **1**, **2**, **3**, **5**, **6** and **7** respectively, attributed to the ligand to metal charge transfer transition bands [17e-17f]. In addition to these bands, Co(III) complexes **1** and **5** exhibit a weak absorption band at ~ 630 nm, consistent with the absorption behavior of Co(III) tris-dipicolyldithiocarbamate complexes [18g]. Further the UV-visible absorption behavior of Cu(II) and Ni(II) complexes are quite similar to those

obtained for bis(2-hydroxyethyl)dithiocarbamate complexes of these transition metals [18h].

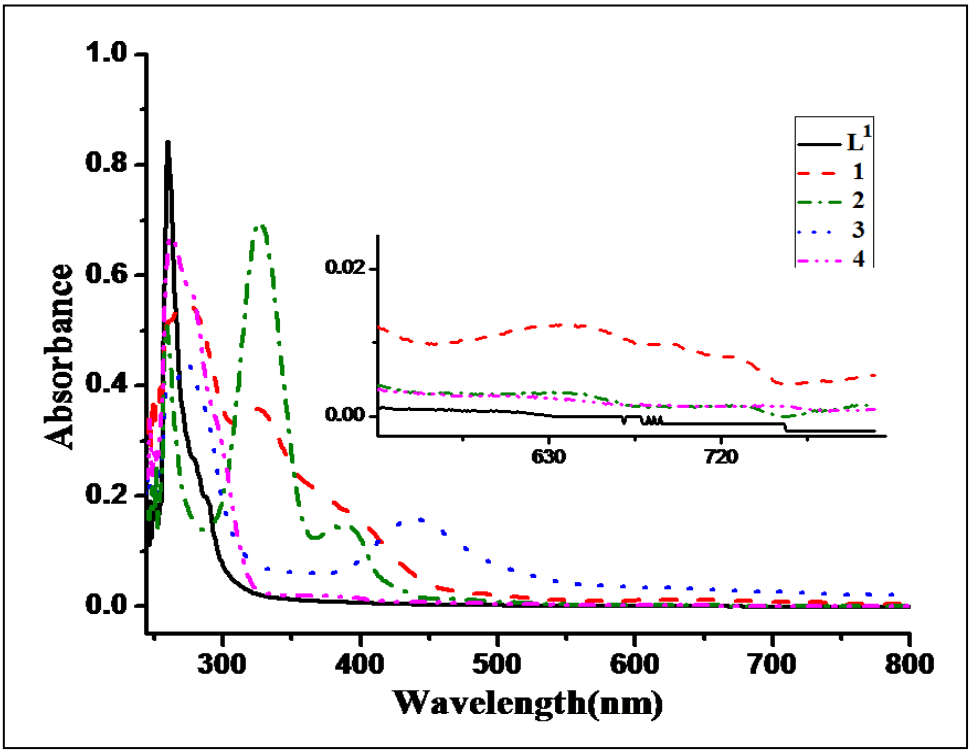

Fig. 1. UV-visible absorption spectra of the ligand precursor (L^1) and mononuclear dithiocarbamate complexes at room temperature in 10^{-5} M DMSO solution.

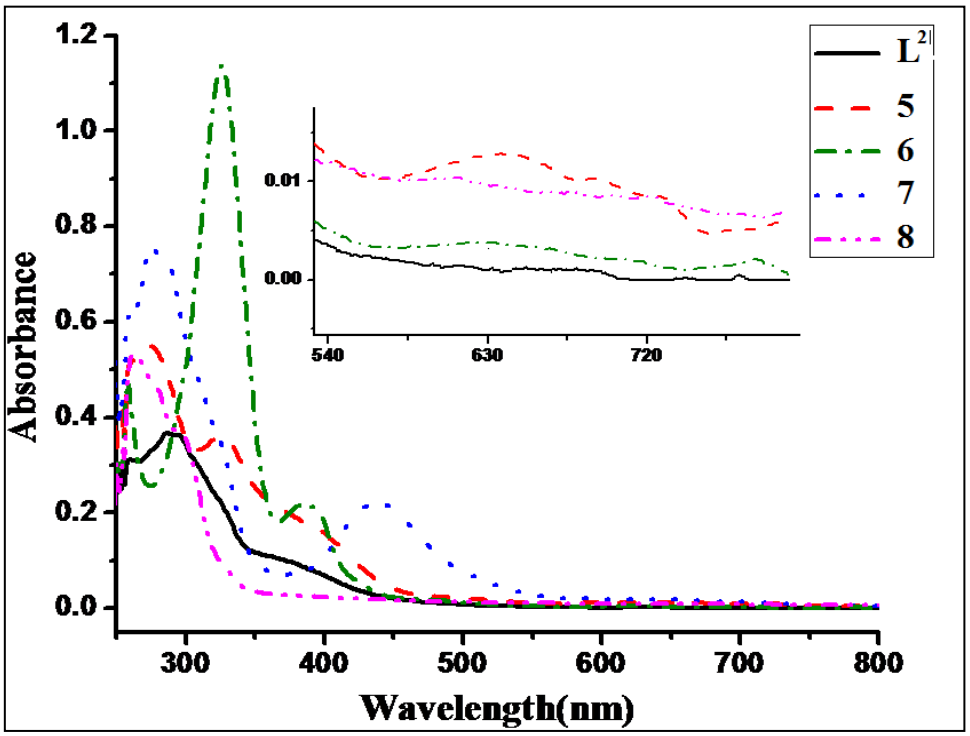

Fig. 2. UV-visible absorption spectra of the ligand precursor (L^2) and mononuclear dithiocarbamate complexes at room temperature in 10^{-5} M DMSO solution.

The Zn(II) complexes 4 and 8 are diamagnetic and are of white colour with featureless electronic spectra presenting a broad absorption at ~263 nm. The magnetic moment values (Table 1) along with UV-visible absorption bands suggest an octahedral environment around Co(III), square planar environment around Ni(II)/ Cu(II) and tetrahedral environment around Zn(II) in their respective mononuclear dithiocarbamate complexes.

Table 1. UV-visible and Fluorescence spectral data of the ligand precursors $\mathbf{L^1}$, $\mathbf{L^2}$ and mononuclear complexes **1-8** in 10^{-5}M DMSO solution.

Entry	λ_{max} nm (ε, L mol^{-1} cm^{-1})	Wave number (cm^{-1})	Transitions	Magnetic moment μ_{eff} (BM)	Fluorescence spectral data	
					λ_{ex} (nm)	λ_{em} (nm)
$\mathbf{L^1}$	260 (84864)	38461	π→π*	--	260	Non-fluorescent
$\mathbf{L^2}$	288 (36601)	34722	π→π*	--	288	353(40) sh π*→π
						443(81) π*→π
1	273 (54975)	36630	π→π*		273	301(68) sh π*→π
	325 (35798)	30769	n→π*	dia		342 (225) π*→π
	398 (16231)	25125	charge transfer			
	635 (15748)					
2	259 (52283)	38610	π→π*			
	326 (69905)	30674	n→π*	dia	259	Non-fluorescent
	388 (14705)	25773	charge transfer			
3	273 (44235)	36630	π→π*	1.89	273	344 (221) π*→π
	439 (16231)	22779	n→π*			
4	263 (66853)	38022	π→π*	dia	263	330(16) π*→π
	277 (56501)	36101	n→π*			
5	273 (55376)	36630	π→π*			
	326 (36182)	30674	n→π*	dia	273	Non-fluorescent
	395 (16918)	25316	charge transfer			
	630 (15873)					
6	259 (47803)	38610	π→π*			
	325 (113518)	30769	n→π*	dia	259	Non-fluorescent
	388 (21838)	25773	charge transfer			
7	274 (75967)	36496	π→π*	1.95	274	Non-fluorescent
	437 (22292)	22883	n→π*			
8	263 (53597)	38022	π→π*		263	348 (343) π*→π
	278 (46477)	35971	n→π*	dia		466 (266) π*→π
						691 (151) π*→π

3B.2.5. Fluorescence emission spectral study

The UV-visible emission properties of the ligand precursor $\mathbf{L^1}$-$\mathbf{L^2}$ and their mononuclear dithiocarbamate complexes **1-8** were investigated at room temperature (298 K) from 10^{-5}M DMSO solution and the spectral data is summarized in Table 1.

The differential emission spectra of these compounds are shown in Figure 2. The precursor L^2 exhibits fluorescence emission bands at 353 and 443 nm upon excitation at λ_{max} = 288 nm but we could not observe any noticeable fluorescence emission for L^1 upon excitation at 260 nm. Complexes **1**, **3** and **8** exhibit maximum fluorescence emissions at 342, 344 and 348 nm upon excitation at 273 (for complex **1** and **3**) and 263 (for complex **8**) with concomitant Stokes shifts of ≈ 69 nm, ≈ 71 nm and ≈ 85 nm. Notably, the behavior of copper (II) complexes are generally fluorescence quenchers, however this copper (II) complex **3** shows very good fluorescence emission behaviour upon excitation of intra ligand charge transfer band. A weak fluorescence emission band at 330 nm with Stokes shifts of ≈ 67 nm is observed for complex **4** upon excitation at 263 nm. Such a trend of fluorescence spectra and concomitant bathochromic shifts of intramolecular charge-transfer emissions by coordination compounds were previously observed in dithiocarbamate complexes [20],dialkoxo-bridged [21] and Salen-type [22] complexes. The appearance of more number of bands upon excitation of a single wavelength (in case of $\mathbf{L^2}$, **1** and **8**) as well as high fluorescence behaviour of the complexes may be attributed to the reduction of photoinduced electron transfer process on complex formation [23].

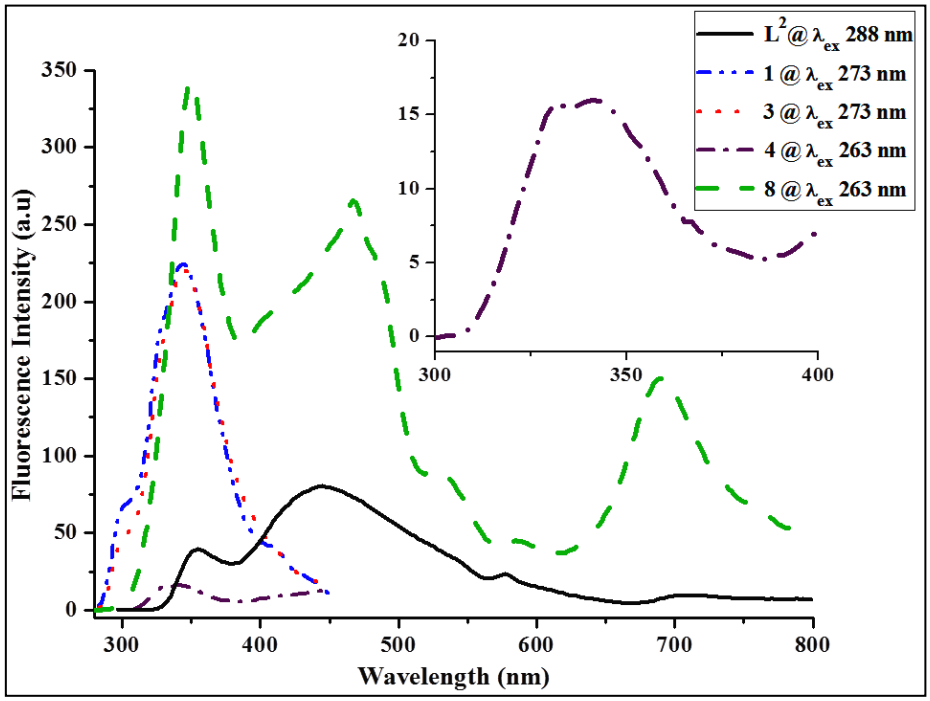

Fig. 3. Fluorescence emission spectra of the ligand precursor L^2 and mononuclear dithiocarbamate complexes at room temperature in 10^{-5} M DMSO solution.

It may be noted that the emission spectra of complexes **1**, **3** and **8** showed similar patterns, i.e. two or more kinds of fluorescence emission bands are appearing by the excitation of single absorption bands (in any case, shoulder is appearing). The complete quenching of fluorescence emissions properties is observed in the mononuclear complexes **2, 5-7**. The exact reason for the fluorescence quenching behavior of these complexes is not clear, however, the literature reports suggest that the fluorescence properties of the compounds is greatly depends upon the molecular arrangements, achieved by means of polymorphism, conformational stiffness of the fluorophore (dihedral angles), intermolecular interactions such as π…π or C-H…π interactions and upon the nature of substituents which can largely affect the photoinduced electron transfer processes [24].

3B.2.6. Thermogravimetric study

All the mononuclear complexes **1-8** were studied for their thermal properties in the temperature ranges from room temperature to 750 ºC. The heating rate was suitably controlled at 10 ºC min^{-1} under an atmosphere of air. The mass losses over a range of temperature, rate of thermal decomposition and the residual masses corresponding to final degradation products are summarized in Table 2. The thermogravimetric plots (Figure 4) suggest that one of the Co(III) complex **1** undergoes thermal degradation in two stages, whereas the other complex **5** exhibits single stage of mass loss and in both the cases mass loss continues even at 750 ºC. On the other hand, the thermal degradation of Ni(II) complexes **2** and **6**, essentially taking place in single stages, giving a broad peak on DTG curves. The TG curves clearly demonstrate that the complex **2** decomposed completely with 77.3% of observed mass loss and a maximum rate of decomposition (0.299 mg min^{-1}) recorded at 250.7 °C on DTG curves. The stable residual mass obtained (22.7 %) corresponds to $NiSO_4$ (calc. 23.9 %) whereas in the case of complex **6**, the thermal degradation is incomplete and a continuous mass loss observed up to 750 ºC. Interestingly, both of the Cu(II) complexes **3** and **7**, exhibit two stages of mass loss on DTG curves with a maximum rate of mass loss at 273.1 and 197.1 ºC respectively, and both the complexes give a stable residual mass of 27.1 % and 23.0 % respectively on TG curves which corresponds to $CuSO_4$. Although, both of the Zn(II) complexes **4** and **8** give three stages of degradation on DTG curves with maximum rate of moss loss at 261.1 ºC, however TG curves reveal that the degradation of complex 4 is completed, giving a

stable residual mass of 22.8 % which corresponds to $ZnSO_4$ (calc 24.7) whereas only 64.3 % of mass loss is observed for complex **8** up to 750 ºC. Interestingly, the thermal decomposition of all the complexes starts before their melting point and the decompositions are accompanied by an endothermic peak on corresponding DTA curves. The formation MSO_4 as a stable residual product during the thermogravimetric analysis of transition metal dithiocarbamate complexes has been previously observed [25].

Table 2. Thermal analysis data of the ligand precursor L^1, L^2 and mononuclear dithiocarbamato complexes **1-8.**

Entry	% Mass loss (Temp. range ºC)	DTG (ºC) (mg min^{-1})	% Residue Calculated (found)	Final product
1	5.9 (60-80) 61.22 (81-720) 67.12 (110-720)	70.0 (0.502), 270.5 (0.842)	-- (32.88)	Incomplete Degradation
2	77.3 (140-730)	250.7 (0.299)	23.9 (22.7)	$NiSO_4$
3	72.9 (141-400)	179.0 (0.129), 273.1 (0.168)	24.5 (27.1)	$CuSO_4$
4	77.2 (150-740)	158.6 (0.080), 261.1 (0.084) 316.2 (0.050)	24.7 (22.8)	$ZnSO_4$
5	65.2 (200-730)	256.9 (0.664)	-- (34.8)	Incomplete degradation
6	63.4 (150-720)	262.1 (0.331)	-- (36.6)	Incomplete degradation
7	77.0 (150-720)	197.1 (0.171), 261.0 (0.143)	21.2 (23.0)	$CuSO_4$
8	24.6 (120-200) 39.7 (201-450)	136.1 (0.072), 158.6 (0.087) 261.1 (0.106)	-- (35.7)	Incomplete degradation

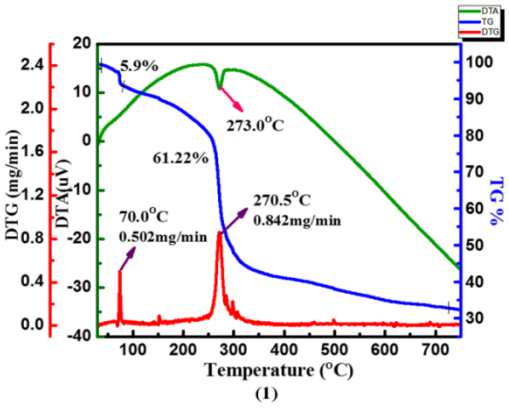

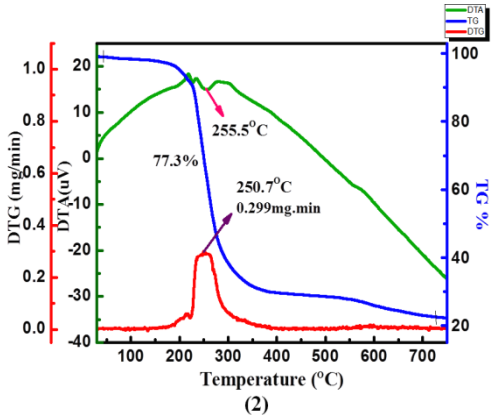

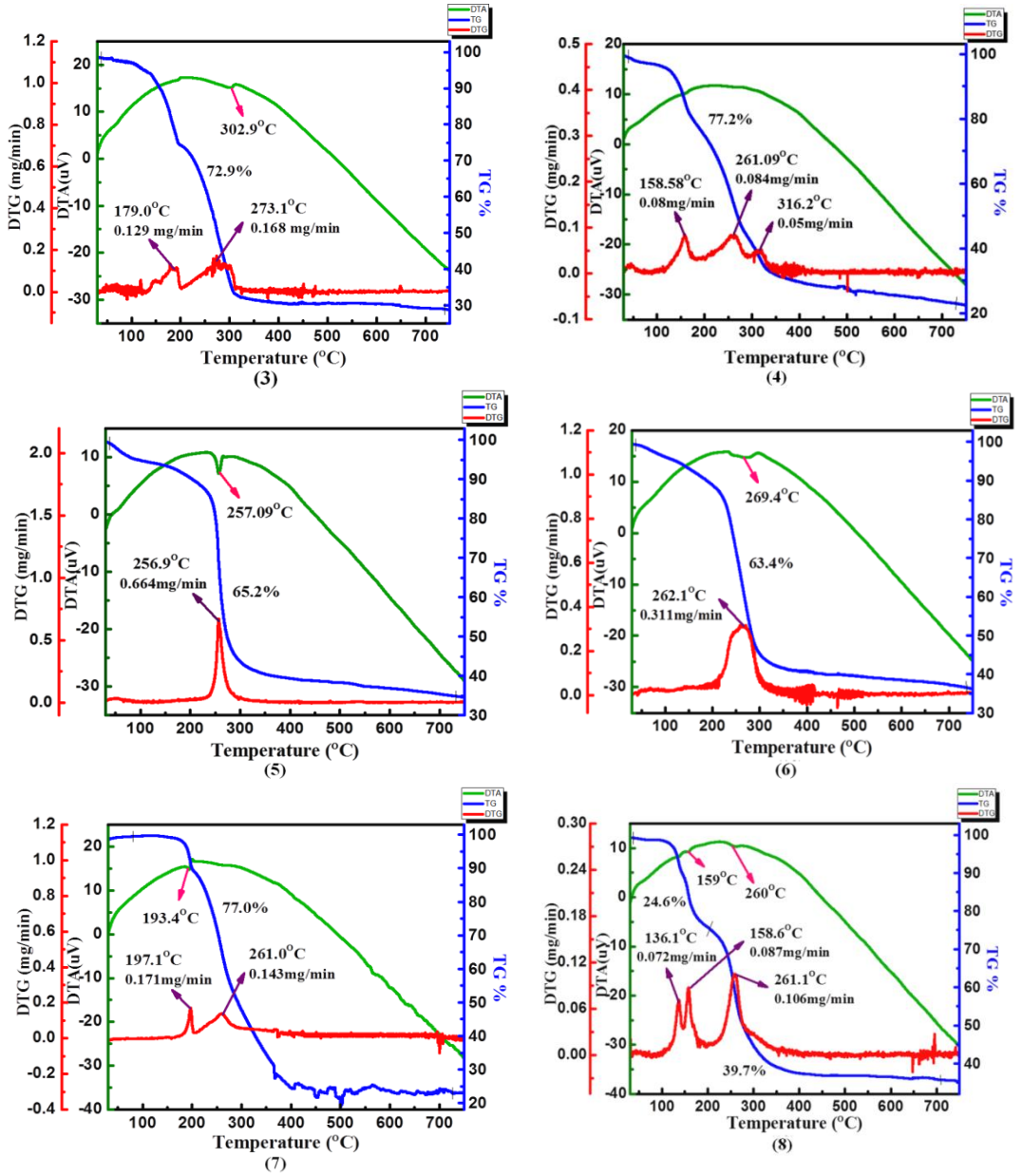

Fig. 4. TG/DTA curves of the Ligand precursor N-[phenylmethylidene]-2-piperazin-1-ylethanamine (L^1), N-[naphthylmethylidene]-2-piperazin-1-ylethanamine (L^2) and mononuclear dithiocarbamato complexes **1-8**.

3B.2.7. Cyclic voltammetry

The electrochemical behavior of the ligand precursor L^2 and its complexes **5-8** in 1.0 mM DMF solutions were investigated in the potential ranges +2.0 to -2.1 V. The experiments were performed with a one-compartment cell having a platinum-disk working electrode, a platinum-wire counter electrode and an Ag/Ag+ (in acetonitrile) reference electrode. Voltammograms were recorded by using anhydrous solutions of the metal complexes in dimethylformamide containing n-Bu_4NPF_6 (0.1 M) as

supporting electrolyte at scan rate of 200 mVs^{-1}. The first electrochemical examination of L^2 clearly demonstrates the reversible redox behavior in the potential range of -0.7 to -1.7 V. The emergence of constant value of peak potential separation ΔE_p and the peak current ratio (i_{pa}/i_{pc} = 1) at all scan rates at 25 ^oC in the electro analysis of L^2 is indicative of its reversible redox behavior. The reduction peak is appeared at Epc = -1.375 in the cathodic scan of the cyclic voltammograms which is apparently associated with the reduction of the imine (-N=C<) group as represented in Scheme 3. The mono anion that is formed upon electroreduction of precursor L^2 is protonated by the solvent to form an amino group which is confirmed by the fact that the reverse scans of the voltammograms show the anodic peak at Epa = -0.979 corresponding to oxidation of the amino group following the first cathodic peak of electroreduction of the precursor L^2. The electroreduction of imine (-N=C<) groups has been previously observed [26] in 1,2-bis[2-(pyridylmethylideneamino) phenylthio]ethanes and their transition metal complexes.

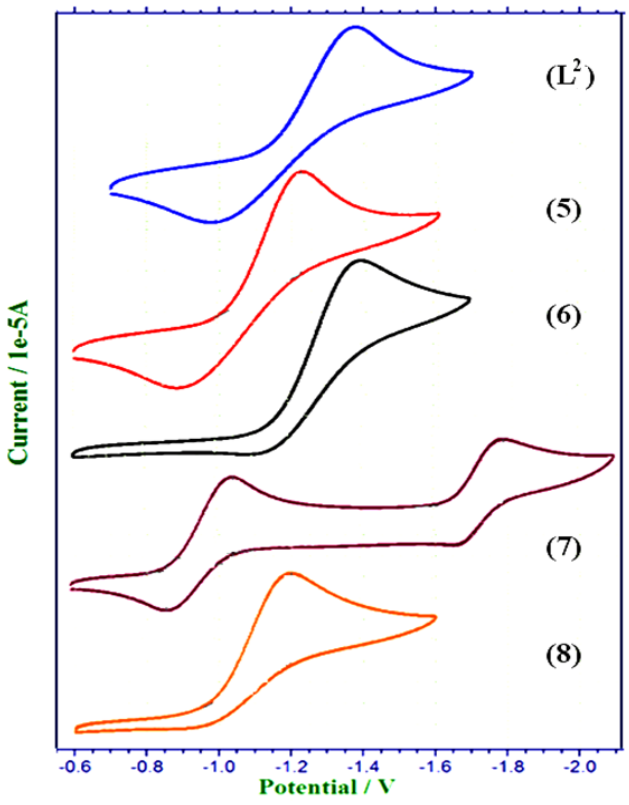

Fig. 5. Cyclic voltammograms of a 1.0 mM solution of the ligand precursor L^2 and mononuclear dithiocarbamate complexes **5-8** in DMF containing 0.1 M tetra-n-butylammonium hexafluorophosphate as the supporting electrolyte.

The voltammograms of all the complexes (except complex **7**) examined in this work, did not display any additional peak, compared to the cyclic voltammograms of L^2, in the cathodic or anodic scan under the similar experimental conditions. This clearly demonstrates that these complexes are primarily electro active with respect to the pendant imine (-N=C<) moieties of the coordinated ligands and the metal centres are present in silent mode. The cyclic voltammograms of the Ni(II) **6** and Zn(II) **8** displays a cathodic peak without corresponding anodic peak and their cathodic peak potential (Epc) was found to be -1.395 and -1.199 V respectively which are indeed very close to the Epc of precursor L^2. The Co(III) **5** complex displays reversible redox behavior, similar to that of L^2 with significant with significantly greater values Ipc and Ipa and slight anodic shift of Eps values associated with imine/amine redox couples, probably due to the presence of tris-dithiocarbamate coordinated ligands. Contrarily, the cyclic voltammogram of Cu(II) complex **7** display additional peaks in the cathodic/anodic scans at less negative potentials (Figure 5), apparently corresponds to the

Cu^{II}/Cu^{I} redox couples. The separation between the anodic and cathodic peaks, DE = Epa – Epc, is 0.183 V which is larger than $\Delta Ep = 0.059/n$ V and the ratio of the current intensity of the cathodic and anodic peaks is 1.65 which is different from unity. This clearly suggests a quasi-reversible process [27] essentially taking place at copper centre. The subsequent peaks which are significantly shifted towards negative potential are associated with the reduction of the imine moiety of coordinated ligand. The increase in the electron density due to initial electroreduction of Cu(II) centre causes a significant cathodic shift of the electroreduction peaks associated with pendant imine moieties of coordinated dithiocarbamate ligands in this complex.

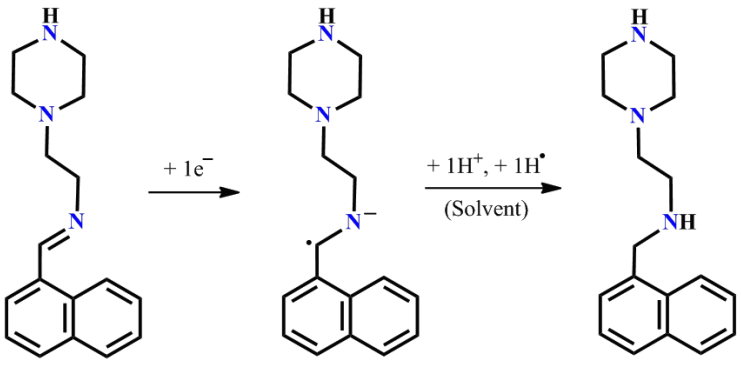

Scheme 3. Electroreduction of imine moiety.

3B.3. Conclusion

A novel series of neutral mononuclear dithiocarbamate complexes of Co(III), Ni(II), Cu(II) and Zn(II) bearing pendant Schiff base moieties were efficiently synthesized through self-assembly process involving the novel amine precursor N-[phenylmethylidene]-2-piperazin-1-ylethanamine (L^1) or N-[naphthylmethylidene]-2-piperazin-1-ylethanamine (L^2) with two equivalents each of CS_2 and corresponding metal acetates. The composition and structure of all complexes are well supported by various physicochemical, spectroscopic data and cyclic voltammetric study. The thermogravimetric study performed on the complexes **1-8** indicates that a majority of complexes is thermally unstable and their degradation starts before their melting points. Complexes **2**, **3**, **4** and **7** degrade completely up to 750 $^{\circ}$C giving a stable residual mass which corresponds to MSO_4. The IR, NMR and cyclic voltammetric studies confirms the presence of pendant Schiff base moieties in all the complexes which added merit to this work. Interestingly, complexes **5**, **6** and **8** are redox active only with respect to the ligand framework, whereas Cu(II) complex **7** is redox active with respect to the metal as well as coordinated ligands. Complex **7** displays a quasi-reversible reduction corresponds to the Cu(II)/Cu(I) redox couples in addition to the reversible electroreduction of the coordinated ligands.

3B.4. Experimental Section

3B.4.1. Materials and measurements

All solvents were purchased from the commercial sources and were freshly distilled prior to use. Reagents such as metal acetates $Co(OAc)_2.4H_2O$, $Ni(OAc)_2.4H_2O$, $Cu(OAc)_2.H_2O$ and $Zn(OAc)_2.2H_2O$ were purchased from Merck and these were used without further purification. Microanalysis (C, H, N, S) were carried out on a Perkin-Elmer 2400 analyzers. ESI MS were obtained from AB SCIEX, 3200 Q TRAP LC/MS/MS system. The m.p.'s of the compounds were recorded in open capillary and are uncorrected. FTIR (KBr pellets) spectra were recorded in the 4000-400 cm^{-1} range using a Perkin-Elmer spectrometer. ^{1}H and ^{13}C NMR on a Bruker 400 MHz spectrometer in DMSO-d6 unless otherwise noted. UV-visible absorption spectra were recorded on a Perkin Elmer Lambda 35 UV-visible spectrophotometer and fluorescence spectra were recorded on JASCO make spectrofluorometer model FP-6300. TGA/DTA plots were obtained using SII TG/DTA 6300 in flowing N_2 with a

heating rate of 10 °C min^{-1}. Electrochemical measurements were performed on a CH Instruments 600C potentiostat, using a Pt disk as the working electrode, Ag/AgCl as the reference electrode and a Pt wire as the counter electrode. Voltammograms were recorded by using anhydrous solutions of the metal complexes in DMF (1.0mM) containing tetra-n-butylammoniumhexafluoro phosphate (0.1M) as supporting electrolyte.

3B.4.2. Synthesis

3B.4.2.1. Synthesis of the N-[phenylmethylidene]-2-piperazin-1-ylethanamine, L^1

This ligand precursor has been synthesized by a modified literature procedures [13c] and this modification was scalable to 95%. To a solution of benzaldehyde (831 mg, 7.84 mmol) in 25 mL of toluene containing 2-3 drops of glacial acetic acid, was added 1-(2-aminoethyl)-piperazine (1000 mg, 7.74 mmol) with rigorous stirring. The reaction mixture was refluxed for 2 hrs using Dean-Stark apparatus. The progress of the reaction was monitored by TLC. The reaction mixture was cooled at room temperature and solvent was evaporated under vacuum, The residue was dissolved in dichloromethane and washed with 5% aqueous sodium carbonate solution followed by distilled water 3-4 times. The dichloromethane layer containing crude product was separated and dried over sodium sulfate for 2 hrs. The solvent was evaporated under vacuum and the product was purified by column chromatography using 3% methanol/ chloroform (v/v) solution as eluent. The product ($\mathbf{L^1}$) was stored under a nitrogen atmosphere and samples were taken for analysis.

$\mathbf{L^1}$: Mw: 217.3. Light yellow solid. Yield: 1597 mg (95%). IR (cm^{-1}): 3275 (N-H), 3061 (C-H), 1644 (C=N), 1449 (C=C). ^{1}H NMR (400 MHz, DMSO-d_6): 2.29 (s, 1H, N-*H*), 2.38–2.49 (t, 6H, CH_2), 2.51–2.55 (m, 2H, CH_2), 2.68–2.70 (t, 2H, CH_2), 3.60–3.69 (m, 2H, CH_2), 7.15–7.17 (t, 1H, *Ph*), 7.40–7.45 (m, 2H, *Ph*), 7.67–7.73 (m, 2H, *Ph*), 8.29 (d,1H, *H*C=N). ^{13}C NMR (400 MHz, DMSO-d_6): δ 161.8 (d,1C, H*C*=N), 136.6, 131.0, 129.1, 128.88, 128.25, 127.87 (all corresponds to the carbons of *Ph*), 59.6, 58.6, 54.4, 53.6, 48.8, 45.8 (all corresponds to the aliphatic carbons). DEPT 135 NMR (400 MHz, DMSO-d_6): δ 161.8 (*H*C=N), 131.0 (CH), 129.1 (CH), 128.88 (CH), 128.25 (CH), 127.87 (CH), 59.57 (CH_2), 58.66 (CH_2), 54.37 (CH_2), 53.67 (CH_2), 45.79 (CH_2).

3B.4.2.2. Synthesis of the N-[naphthylmethylidene]-2-piperazin-1-ylethanamine, L^2

To a solution of naphthaldehyde (1223 mg, 7.84 mmol) in 25 mL of toluene containing 2-3 drops of glacial acetic acid, was added 1-(2-aminoethyl)-piperazine (1000 mg, 7.74 mmol) with rigorous stirring. The reaction mixture was refluxed for 2 hrs using Dean-Stark apparatus. The progress of the reaction was monitored by TLC. The reaction mixture was cooled at room temperature and solvent was evaporated under vacuum, The residue was dissolved in dichloromethane and washed with 5% aqueous sodium carbonate solution followed by distilled water 3-4 times. The dichloromethane layer containing crude product was separated and dried over sodium sulfate for 2 hrs. The solvent was evaporated under vacuum and the product was purified by column chromatography using 6% methanol/ chloroform (v/v) solution as eluent. The product ($\mathbf{L^2}$) was stored under nitrogen atmosphere and samples were taken for analysis.

$\mathbf{L^2}$: Mw: 267.4. Light brown solid. Yield: 2155 mg (96%). IR (cm^{-1}): 3195 (N-H), 2996 (C-H), 1649 (C=N), 1503, 1456 (C=C). ^{1}H NMR (400 MHz, DMSO-d_6): δ 3.15 (s, 1H, N-*H*), 2.27 (s, 2H, *CH*$_2$), 2.49–2.51 (t, 2H, *CH*$_2$), 2.56–2.62 (t, 2H, *CH*$_2$), 2.68–2.70 (t, 2H, *CH*$_2$), 3.68–3.71 (t, 2H, *CH*$_2$), 3.77–3.80 (t, 2H, *CH*$_2$), 7.14–7.16 (m, 1H, *Ph*), 7.45–7.60 (m, 3H, *Ph*), 7.81–8.01 (m, 3H, *Ph*), 8.94 (d, 1H, *H*C=N). ^{13}C NMR (400 MHz, DMSO-*d6*): δ 162.0 (H*C*=N), 137.7, 133.9, 131.7, 131.0, 129.3, 128.9, 128.2, 127.4, 126.6, 125.7 (all corresponds to *naphthyl group*) 59.7, 58.9, 55.4, 54.6, 53.7, 45.9 (all corresponds to aliphatic carbons). DEPT 135 NMR (400 MHz, DMSO-d_6): δ 162.0 (H*C*=N), 131.2 (*C*H), 129.3 (*C*H), 128.9 (*C*H), 128.6 (*C*H), 127.4 (*C*H), 126.5 (*C*H), 125.7 (*C*H), 59.5 (*C*H$_2$), 58.9 (*C*H$_2$), 55.4 (*C*H$_2$), 54.6 (*C*H$_2$), 53.4 (*C*H$_2$), 51.5 (*C*H$_2$).

3B.4.2.3. General synthesis of mononuclear [M{κ^2S,S-S_2C-piperazine-C_2H_4N=C(R)}$_n$] Complexes, 1-8

In a typical procedure, N-[phenylmethylidene]-2-piperazin-1-ylethanamine (434.6 mg, 2.0 mmol) or N-[naphthylmethylidene]-2-piperazin-1-ylethanamine (534.8 mg, 2.0 mmol) and excess amount of CS_2 *ca* (0.5 mL, 8.32 mmol) were added in 20 mL of Et_3N solvent. The reaction mixture was allowed to stir for 1 hr at room temperature wherein a change in colour from colourless to yellow was observed. To this mixture, $Co(OAc)_2.4H_2O$ (168 mg, 0.66 mmol), $Ni(OAc)_2.4H_2O$ (248 mg, 1.0 mmol),

$Cu(OAc)_2.H_2O$ (201 mg, 1.0 mmol) or $Zn(OAc)_2.2H_2O$ (220 mg, 1.0 mmol) was added with rigorous stirring and the reaction was allowed to continue for 6 h at room temperature. The residue was filtered in a glass sintered crucible and washed several times with distilled water, followed by n-hexane and diethyl ether to yield the products **1-8** which were dried under vacuum and stored under nitrogen atmosphere before samples were taken for analysis. This synthetic methodology is outlined in Scheme **2**.

[Co{κ^2S,S-S_2C-piperazine-C_2H_4N=C(Ph)}$_3$] (1): Mw: 936.2. Green solid. Yield: 549.9 mg (89%). Mp: 245-250 (dec). Anal. Calcd. for $C_{42}H_{54}N_9S_6Co$ (%): C, 53.88; H, 5.81; N, 13.46; S, 20.55. Found: C, 53.97; H, 5.71; N, 13.52; S, 20.63. IR (cm^{-1}): 2935 (C-H), 1636 (C=N), 1492 (N-CS_2), 1433 (C=C), 999 (C-S). NMR data could not be recorded due to poor solublility in DMSO even in acidic medium.

[Ni{κ^2S,S-S_2C-piperazine-C_2H_4N=C(Ph)}$_2$] (2): Mw: 643.6. Green solid. Yield: 559.9 mg (87%). Mp: 221-225 (dec). Anal. Calcd. for $C_{28}H_{36}N_6S_4Ni$ (%): C, 52.25; H, 5.64; N, 13.06; S, 19.93. Found: C, 52.39; H, 5.71; N, 13.13; S, 20.01. IR (cm^{-1}): 3057 (C-H), 1639 (C=N), 1503 (N-CS_2), 1430s (C=C), 996 (C-S). ^{1}H NMR (400 MHz, DMSO-d_6 + D_2O+HCl ≈ 3 p^H): 3.2 (t, 2H, CH_2), 3.4 (t, 6H, CH_2), 3.5 (s, 4H, CH_2), 7.5–7.54 (t, 2H, *Ph*), 7.6 (d, 1H, *Ph*), 7.8 (d, 2H, *Ph*), 9.8 (d, 1H, *H*C=N). ^{13}C NMR (400 MHz, DMSO-*d6*+ D_2O+HCl ≈ 3 p^H): δ 210.6 (-N*C*S_2), 194.6 (H*C*=N), 192.9, 135.3, 129.9, 129.6, 53.2, 48.8, 41.7, 34.5. DEPT 135 NMR (400 MHz, DMSO-d_6+ D_2O+HCl ≈ 3 p^H): δ 194.6 (H*C*=N), 135.3 (*C*H), 129.9 (*C*H), 129.6 (*C*H), 53.2 (CH_2), 48.8 (CH_2), 41.7 (CH_2), 34.4 (CH_2).

[Cu{κ^2S,S-S_2C-piperazine-C_2H_4N=C(Ph)}$_2$] (3): Mw: 648.4. Brown solid. Yield: 525.2 mg (81%). Mp: 215-223 (dec). Anal. Calcd. for $C_{28}H_{36}N_6S_4Cu$ (%): C, 51.86; H, 5.60; N, 12.96; S, 19.78. Found: C, 51.92; H, 5.75; N, 13.09; S, 19.86. IR (cm^{-1}): 2942 (C-H), 1642 (C=N), 1490s (N-CS_2), 1432s (C=C), 997 (C-S).

[Zn{κ^2S,S-S_2C-piperazine-C_2H_4N=C(Ph)}$_2$] (4): Mw: 650.3. White solid. Yield: 585.2 mg (90%). Mp: 238-243 (dec). Anal. Calcd. for $C_{28}H_{36}N_6S_4Zn$ (%): C, 51.72; H, 5.58; N, 12.92; S, 19.72. Found: C, 51.79; H, 5.64; N, 12.97; S, 19.79. IR (cm^{-1}): 2938 (C-H), 1643 (C=N), 1480s (N-CS_2), 1431s (C=C), 997 (C-S). ^{1}H NMR (400 MHz, DMSO-d_6): 3.36 (t, 6H, CH_2), 3.73 (t, 4H, CH_2), 4.0 (s, 2H, CH_2), 7.44–7.45 (t, 2H, *Ph*), 7.59–7.63 (t, 1H, *Ph*), 7.72–7.74 (dd, 1H, *Ph*), 7.90–7.92 (d, 1H, *Ph*), 8.36 (s, 1H, *H*C=N). ^{13}C NMR (400 MHz, DMSO-d_6): δ 193.6, 164.2, 135.0, 129.9, 129.6,

52.5, 51.2, 46.1. DEPT 135 NMR (400 MHz, DMSO-d_6): δ 164.4 (H*C*=N), 135.0 (*C*H), 129.9 (*C*H), 129.6 (*C*H), 52.5 (*C*H_2), 51.2 (*C*H_2), 47.5 (*C*H_2) 46.1 (*C*H_2). ESI-MS: m/z 651.1 $[M+H]^+$.

[Co{κ^2S,S-S_2C-piperazine-C_2H_4N=C(Naph)}$_3$] (5): Mw: 1086.4. Green solid. Yield: 602.3 mg (84%). Mp: 265-271 (dec). Anal. Calcd. for $C_{54}H_{60}N_9S_6Co$ (%): C, 59.70; H, 5.57; N, 11.60; S, 17.71. Found: C, 59.77; H, 5.63; N, 11.74; S, 17.85. IR (cm^{-1}): 2932 (C-H), 1640 (C=N), 1491s (N-CS_2), 1433s (C=C), 1003 (C-S). NMR could not be recorded due to poor solubility in DMSO even after acidification.

[Ni{κ^2S,S-S_2C-piperazine-C_2H_4N=C(Naph)}$_2$] (6): Mw: 743.7. Green solid. Yield: 639.5 mg (86%). Mp: 230-234 (dec). Anal. Calcd. for $C_{36}H_{40}N_6S_4Ni$ (%): C, 58.14; H, 5.42; N, 11.30; S, 17.25. Found: C, 58.23; H, 5.49; N, 11.38; S, 17.32. IR (cm^{-1}): 3043 (C-H), 1642 (C=N), 1509s (N-CS_2), 1437s (C=N), 994 (C-S). ESI-MS: m/z 745.0 $[M+H]^+$. NMR could not be recorded due to poor solubility in DMSO even after acidification.

[Cu{κ^2S,S-S_2C-piperazine-C_2H_4N=C(Naph)}$_2$] (7): Mw. 748.5. Brown solid. Yield: 621.2 mg (83%). Mp: 205-212 (dec). Anal. Calcd. for $C_{36}H_{40}N_6S_4Cu$ (%): C, 57.76; H, 5.39; N, 11.23; S, 17.13. Found: C, 57.82; H, 5.47; N, 11.30; S, 17.21. IR (cm^{-1}): 3049 (C-H), 1641 (C=N), 1486s (N-CS_2), 1432s (C=C), 995 (C-S).

[Zn{κ^2S,S-S_2C-piperazine-C_2H_4N=C(Naph)}$_2$] (8): Mw. 750.4. White solid. Yield: 675.3 mg (91%): Mp: 208-217 (dec). Anal. Calcd. for $C_{36}H_{40}N_6S_4Zn$ (%): C, 57.62; H, 5.37; N, 11.20; S, 17.09. Found: C, 57.75; H, 5.43; N, 11.35; S, 17.20. IR (cm^{-1}): 3047 (C-H), 1640 (C=N), 1474s (N-CS_2), 1429s (C=C), 998 (C-S). ^{1}H NMR (400 MHz, DMSO-d_6) (ppm): δ 2.62 (t, 8H, *C*H_2), 2.89 (t, 4H, *C*H_2), 3.56 (t, 4H, *C*H_2), 4.80 (m, 8H, *C*H_2), 7.58–7.64 (m, 4H, *Ph*), 7.67–7.77 (m, 2H, *Ph*), 7.91–7.93 (m, 2H, *Ph*), 7.98–8.08 (m, 4H, *Ph*), 8.20–8.22 (d, 1H, *Ph*), 8.29–8.31 (m, 1H, *Ph*), 9.03 (d, 1H, *H*C=N), 9.17 (d, 1H, *H*C=N). ^{13}C NMR (400 MHz, DMSO-d_6): δ 194.5, 166.4, 137.7, 136.0, 134.0, 129.3, 127.3, 125.8, 53.1, 51.1, 49.6, 46.1. DEPT 135 NMR (400 MHz, DMSO-d_6): δ 162.2 (*H*C=N), 135.5 (*C*H), 132.5 (*C*H), 131.0 (*C*H), 129.4 (*C*H), 127.6 (*C*H), 126.6 (*C*H), 125.9 (*C*H), 124.9 (*C*H), 123.4 (*C*H), 59.3 (*C*H_2), 58.1 (*C*H_2), 52.8 (*C*H_2), 51.0 (*C*H_2), 46.1 (*C*H_2).

3B.5. References

1. (a) Coucouvanis, D.; *Prog. Inorg. Chem*. **1979**, *26*, 301; (b) Tiekink, E. R. T.; Haiduc, I. *Prog. Inorg. Chem*. **2005**, *54*, 127; (c) Bousseau, M.; Valade, L.; Legros, J. P.; Cassoux, P.; Garbaukas, M.; Interrante, L.V. *J. Am. Chem. Soc.* **1986**, *108*, 1908; (d) Coomber, D.; Beljonne, A. T.; Friend, R. H.; Bredas, J. L.; Charlton, A.; Robertson, N.; Underhill, A. *Nature*, **1996**, *380*, 144; (e) Singh, N.; Singh, V. K. *Trans. Met. Chem*. **2001**, *26*, 435; (f) Singh, N.; Singh, V. K. *Trans. Met. Chem*. **2002**, *27*, 359; (g) Kobayashi, A.; Fujiwara, E.; Kobayashi, H. *Chem. Rev*. **2004**, *104*, 5243.
2. (a) Singh, V.; Chauhan, R.; Gupta, A. N.; Kumar, V.; Drew, M. G. B.; Bahadur, L.; Singh, N. *Dalton Trans*. **2014**, *43*, 4752; (b) Singh, N.; Kumar, A.; Prasad, R.; Molloy, K. C.; Mahon, M. F. *Dalton Trans*. **2010**, *39*, 2667; (c) Wilton-Ely, J. D. E. T.; Solanki, D.; Knight, E. R.; Holt, K. B.; Thompson, A. L.; Hogarth, G. *Inorg. Chem*. **2008**, *47*, 9642; (d) Wilton-Ely, J. D. E. T.; Solanki, D.; Hogarth, G. *Eur. J. Inorg. Chem.* **2005**, 4027; (e) Wong, W. W. H.; Cookson, J.; Evans, E. A. L.; McInnes, E. J. L.; Wolowska, J.; Maher, J. P.; Bishop, P.; Beer, P. D. *Chem. Commun.* **2005**, 2214.
3. (a) Yoshikawa, Y.; Adachi, Y.; Sukurai, H. *Life Sciences*, **2007**, *80*, 759; (b) Ozkirimli, S.; Apak, T. I.; Kiraz, M.; Yegenoglu, Y. *Arch. Pharm. Res.* **2005**, *28*, 1213; (c) Alverdi, V.; Giovagnini, L.; Marzamo, C.; Seraglia, R.; Bettio, F.; Sitran, S.; Graziani, R.; Fregona, D. *J. Inorg. Biochem*. **2004**, *98*, 1117.
4. (a) Fan, D.; Afzaal, M.; Malik, M. A.; Nguyen, C. Q.; Brien, P. O.; Thomas, P. J. *Coord. Chem. Rev*. **2007**, *251*, 1878; (b) Maneeprakorn, W.; Malik, M. A.; O'Brien, P. *J. Mater. Chem*. **2010**, *20*, 2329; (c) Revaprasadu, N.; Malik, M. A.; O'Brien, P.; Wakefield, G. *J. Mater. Res.*,**1999**, *14*, 3237; (d) Malik, M. A.; Motevalli, M.; O'Brien, P. *lnorg. Chem.* **1995**, *34*, 6223; (e) Mallk, M. A.; Motevalli, M.; Walsh, J. R.; O'Brien, P. *Organometallics*, **1992**, *11*, 3136; (f) Memon, A. A.; Afzaal, M.; Malik, M. A.; Nguyen, C. Q.; O'Brien, P.; Raftery, J. *Dalton Trans.* **2006**, 449; (g) Mlowe, S.; Lewis, D. J.; Malik, M.; Raftery, J.; Mubofu, E. B.; O'Brienb, P.; Revaprasadu, N. *New J. Chem.* **2014**, *38*, 6073.
5. (a) Sharma, A. K. *Thermochim. Acta*, **1986**, *104*, 339; (b) Hill, J. O.; Murray, J. P.; Patil, *Rev.* K. C. *Inorg. Chem*. **1994**, ***14***, 363.
6. Onwudiwe, D. C.; Ajibade, P. A. *Int. J. Mol. Sci*. **2011**, *12*, 1964.

7. (a) Memon, A. A.; Afzaal, M.; Malik, M. A.; Nguyen, C. Q.; O'Brien, P.; Raftery, J. *Dalton Trans*. **2006**, 4499; (b) kumaar, S. S.; Selvi, T. R. *Synth. React. Inorg. Met.-Org. Nano-Met. Chem*. **2008**, *38*, 710.
8. Anastasiadis, C.; Hogarth, G.; W.-Ely, J. D. E. T. *Inorg. Chim. Acta*, **2010,** *363*, 3222. *and the references cited in*.
9. (a) Wilton-Ely, J. D. E. T. *Dalton Trans*. **2008**, 25; (b) Knight, E. R.; Leung, N. H.; Thompson, A. L.; Hogarth, G.; Wilton-Ely, J. D. E. T. *Inorg. Chem*. **2009**, *48*, 3866.
10. Cookson, J.; Beer, P. D. *Dalton Trans*. **2007**, 1459.
11. Auzeloux, P.; Papon, J.; Masnada, T.; Borel, M.; Moreau, M. F.; Veyre, A.; Pasqualini, R.; Madelmont, J. C. *J. Label. Compd. Radiopharm*. **1999**, *42*, 325.
12. (a) Jones, M. M.; Singh, P. K.; Jones, S. G.; Holscher, M. A. *Pharamcol. Toxicol*. **1991**, *68*, 115; (b) Jones, M. M.; Cherian, M. G.; Singh, P. K.; Basinger, M. A.; Jones, S. G. *Toxicol. Appl. Pharmacol.* **1991**, *110*, 241.
13. (a) Choudhary, P.; Kumar, R.; Verma, K. *Bioorg. Med. Chem*. **2006**, *14*, 1819; (b) Upadhayaya, R. S.; Sinha, N.; Jain, S.; Kishore, N.; Chandra, R.; Arora, S. K. *Bioorg. Med. Chem.* **2004**, *12*, 2225; (c) Shingade, S. G.; Bari, S. K. B. *Med Chem Res*. **2013**, *22*, 699 .
14. Zagidullin, R. N. *Chem. Heterocycl. Compd.* **1989**, *25*, 1275.
15. Anastasiadis, C.; Hogarth, G.; Wilton-Ely, J. D. E. T. *Inorganica Chimica Acta*, **2010**, *363*, 3222.
16. (a) Mamba, S. M.; Mishra, A. K.; Mamba, B. B.; Njobeh, P. B.; Dutton, M. F.; Kankeu, E. F. *Spectrochimica Acta Part A*, **2010**, *77*, 579; (b) Verma, S. K.; Singh, V. K. *Polyhedron*, **2014**, *76*, 1.
17. Valarmathi, P.; Thirumaran, S.; Ragi, P.; Ciattini, S. *J. Coord. Chem.* **2011**, *64*, 4157.
18. (a) Shyamala, B. S.; Lakshmi, P. V. A.; Raju. V. J. *J. Sci. Res*. **2010**, *2*, 525; (b) Riveros, P. C.; Perilla, I. C.; Poveda, A.; Keller, H. J.; Pritzkow, H. Polyhedron, **2000**, *19*, 2327; (c) B. F. G.; Johnson, K. H.; Al-Obalidi, J. A. Mecleverty, *J. Am. Chem. Soc. A*, **1969**, *19*, 1668; (d) Anderson, R. J.; Bendell, D. J.; Groundwater, P. W. Organic Spectroscopic Analysis; RSC: Cambridge, UK 2004; (e) Wong,; W. W. H.; Phipps, D. E.; Beer, P. D. *Polyhedron* **2004**, *23*, 2821; (f) Gölcü, A.; Yavuz, P.; *Russ. J. Coord. Che*m. **2008**, *34*, 106; (g) Vanthoeun, K.; Yamazaki,

H.; Suzuki, T.; Kita, M. *J. Coord. Che*m. **2013**, *66*, 2378; (h) Jeffrey, N. K.; James, F. S. *Anal. Chem.* **1987**, *59*, 703.

19. Kadu, R.; Singh, V. K.; Verma, S. K.; Raghavaiah, P.; Shaikh, M. M. *J. Mol. Struct*. **2013**, *1033*, 298.
20. Verma, S. K.; Kadu, R.; Singh, V. K. *Synth. React. Inorg. Met.-Org. Nano-Met. Chem*. **2014**, *44*, 441.
21. Chai, L. -Q.; Wang, G.; Sun, Y. -X.; Dong, W. -K.; Zhao, L.; Gao, X. -H. *J. Coord. Chem*. **2012**, *65*, 1621.
22. Pandey, R.; Kumar, P.; Singh, A. K.; Shahid, M.; Li, P. Z.; Singh, S. K.; Xu, Q.; Misra, A.; Pandey, D. S. *Inorg. Chem*. **2011**, *50*, 3189.
23. Sreedaran, S.; Bharathi, K. S.; Rahiman, A. K.; Jagadish, L.; Kaviyarasan, V.; Narayanan, V. *Polyhedron* **2008**, *27*, 2931.
24. (a) Mizobe, Y.; Hinoue, T.; Yamamoto, A.; Hisaki, I.; Miyata, M.; Hasegawa, Y.; Tohnai, N. *Chem. Eur. J*. **2009**, *15*, 8175; (b) Lee, K. -H.; Choi, C. -S.; Jeon, K. -S. *J. Photosci*. **2002**, *9*, 71; (c) Martens, S. C.; Zschieschang, U.; Wadepohl, H.; Klauk, H.; Gade, L. H. *Chem. Eur. J*. **2012**, *18*, 3498; (d) Valdés, A. C.; Pina-Luis, G.;. Rivero, I. A *J. Mex. Chem. Soc*. **2007**, *51*, 87; (e) Madrigal, D.; Pina-Luis, G.; Rivero, I. A. *J. Mex. Chem. Soc*. **2006**, *50*, 175.
25. Ali, B. F.; Al-Akramawi, W. S.; Al-Obaidi, K. H.; Al-Karboli, A. H. A. *Thermochimica Acta* **2004**, *419*, 39.
26. Beloglazkina, E. K.; Majouga, A. G.; Moiseeva, A. A.; Yudin, I. V.; Moiseev, F. S.; Shmatova, O. I.;. Zyk, N. V. *Russ. Chem. Bul., Int. Ed.* **2008**, *57*, 358.
27. Lamour, E.; Routier, S.; Bernier, J. -L.; Catteau, J. -P.; Bailly, C.; Vezin, H. *J. Am. Chem. Soc.* **1999**, *121*, 1862.

3B.6. Spectra

3B.6.1. IR Spectra

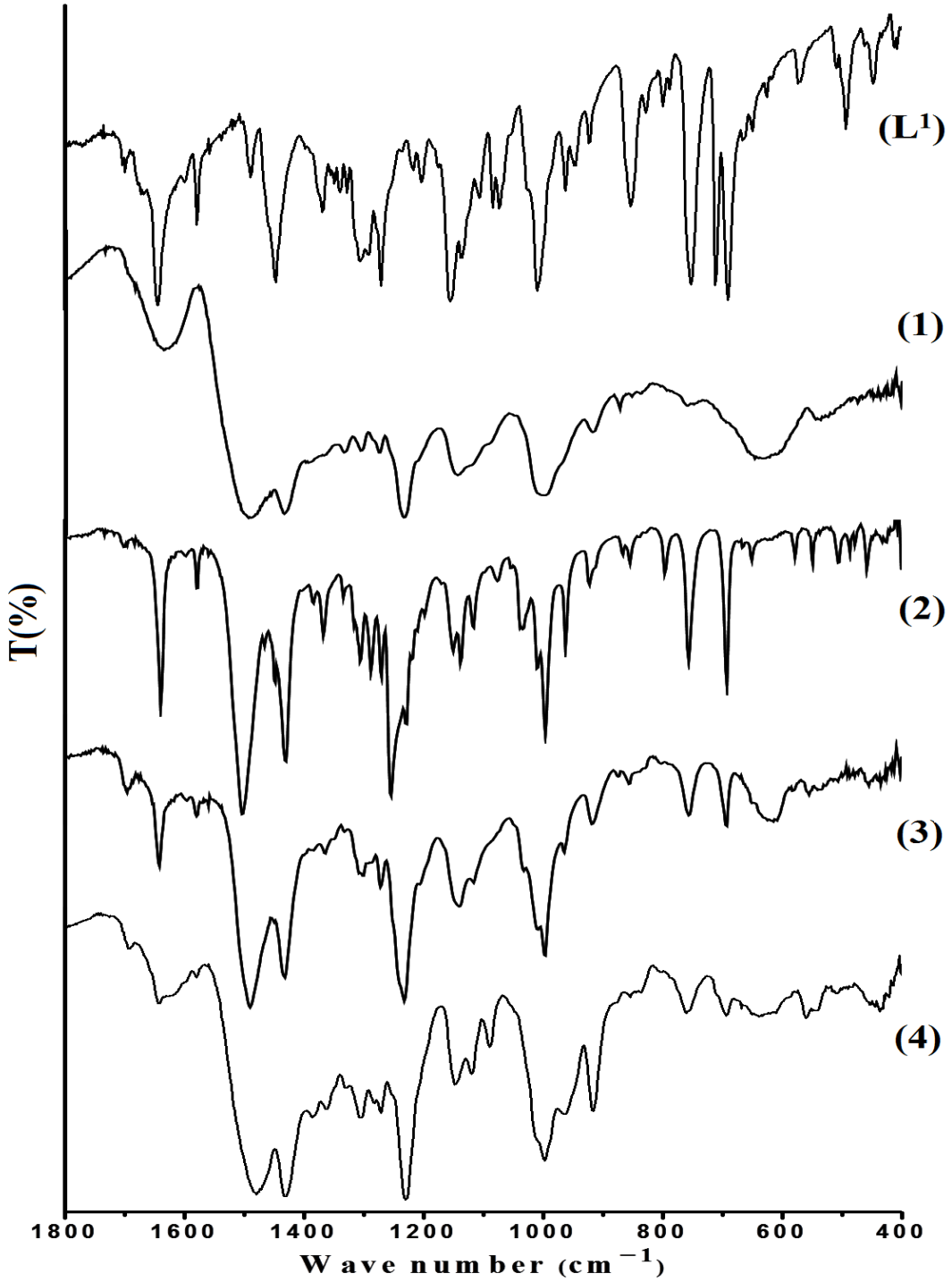

Figure S1. IR Spectra of N-[phenylmethylidene]-2-piperazin-1-ylethanamine (L^1) and compounds 1−4.

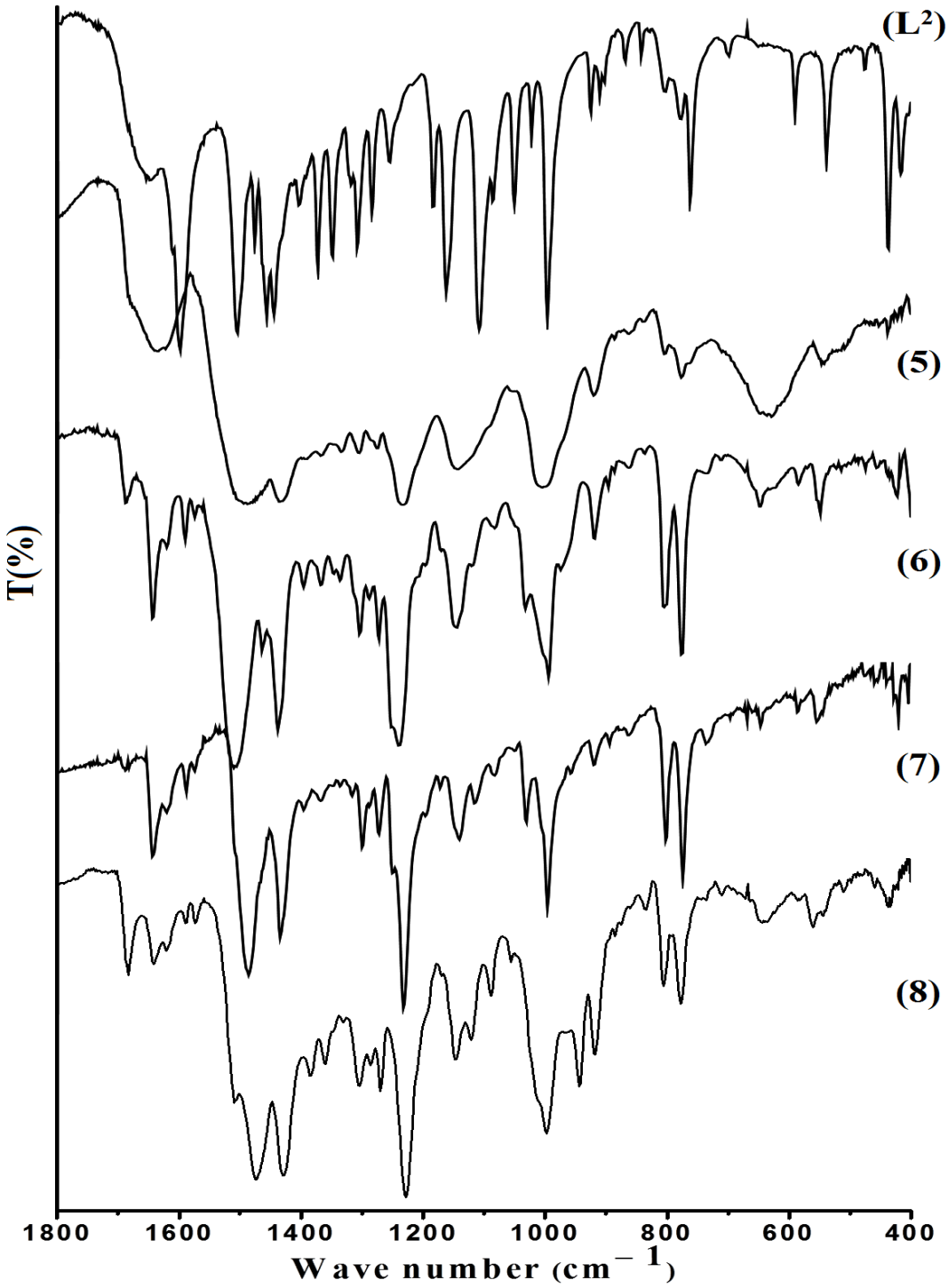

Figure S2. IR Spectra of or N-[naphthylmethylidene]-2-piperazin-1-ylethanamine (L^2) compounds 5−8.

3B.6.2. NMR spectra

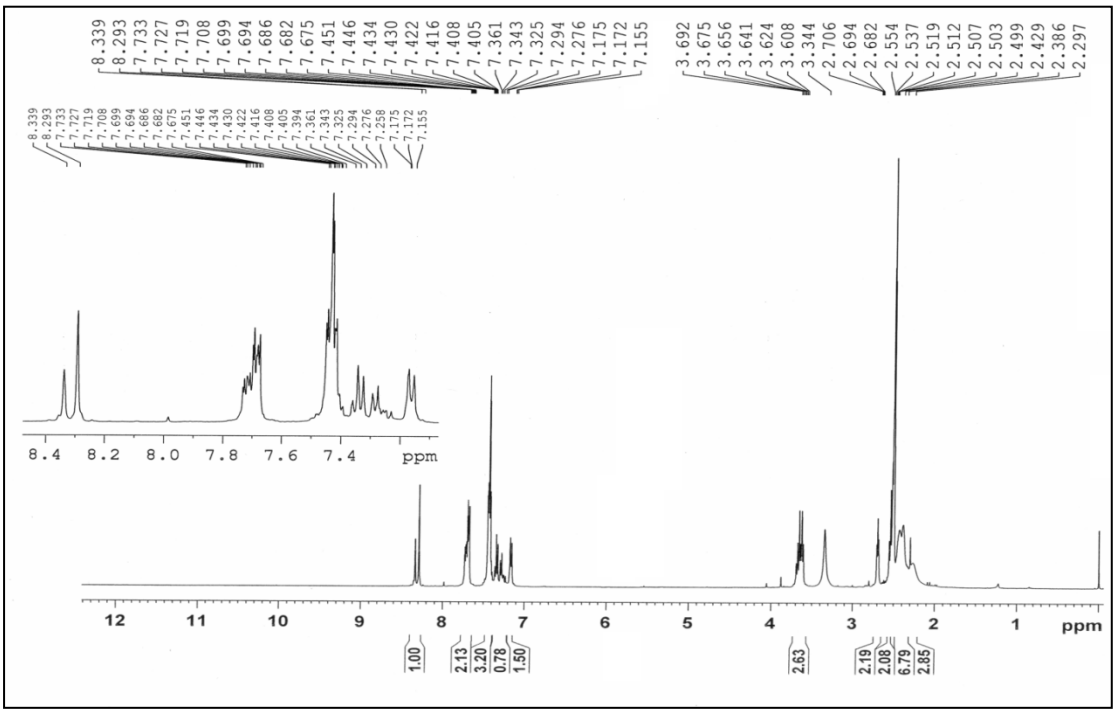

Figure S3. ^{1}H NMR spectrum of N-[phenylmethylidene]-2-piperazin-1-ylethanamine (L^1).

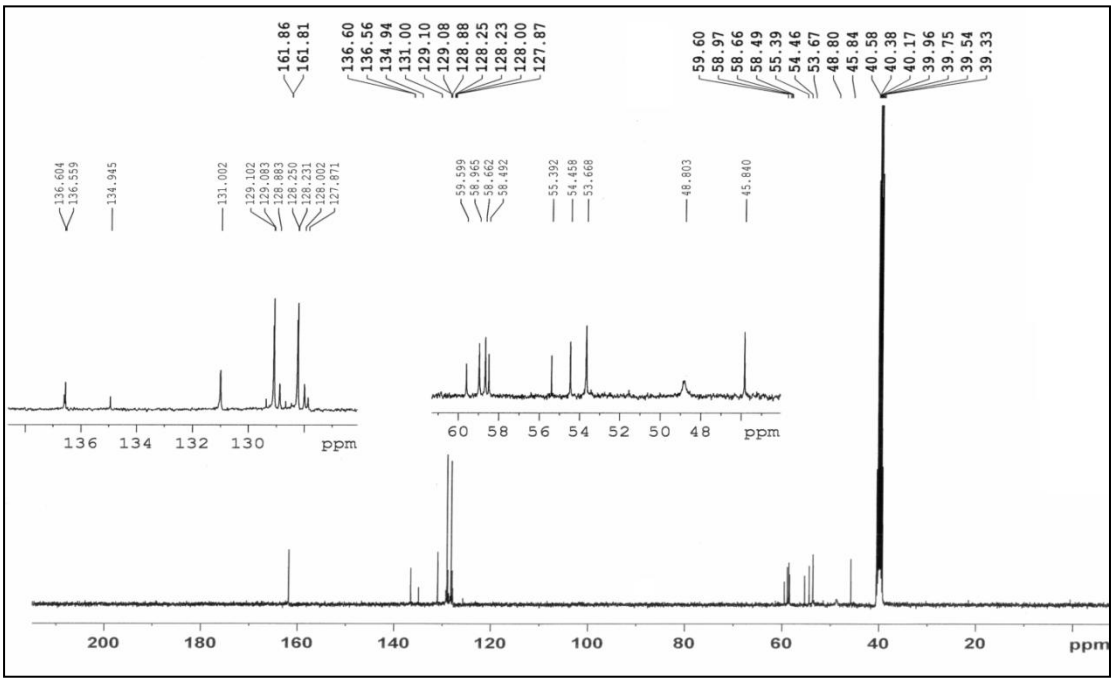

Figure S4. ^{13}C NMR spectrum of N-[phenylmethylidene]-2-piperazin-1-ylethanamine (L^1).

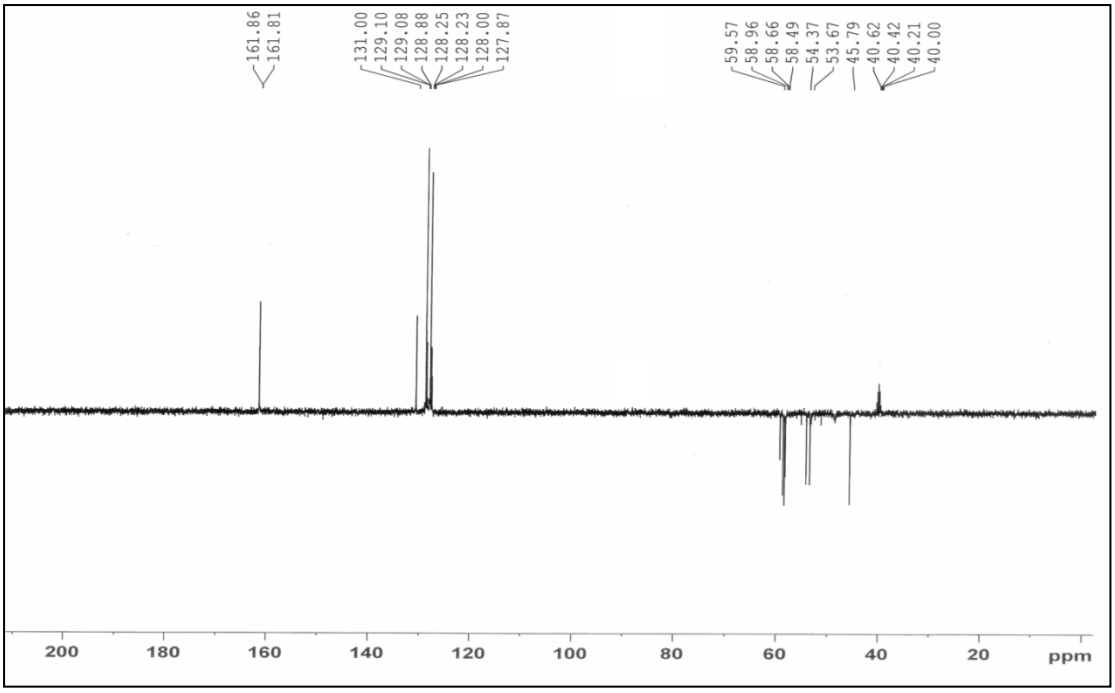

Figure S5. ^{13}C DEPT 135 NMR spectrum of N-[phenylmethylidene]-2-piperazin-1-ylethanamine (L^1).

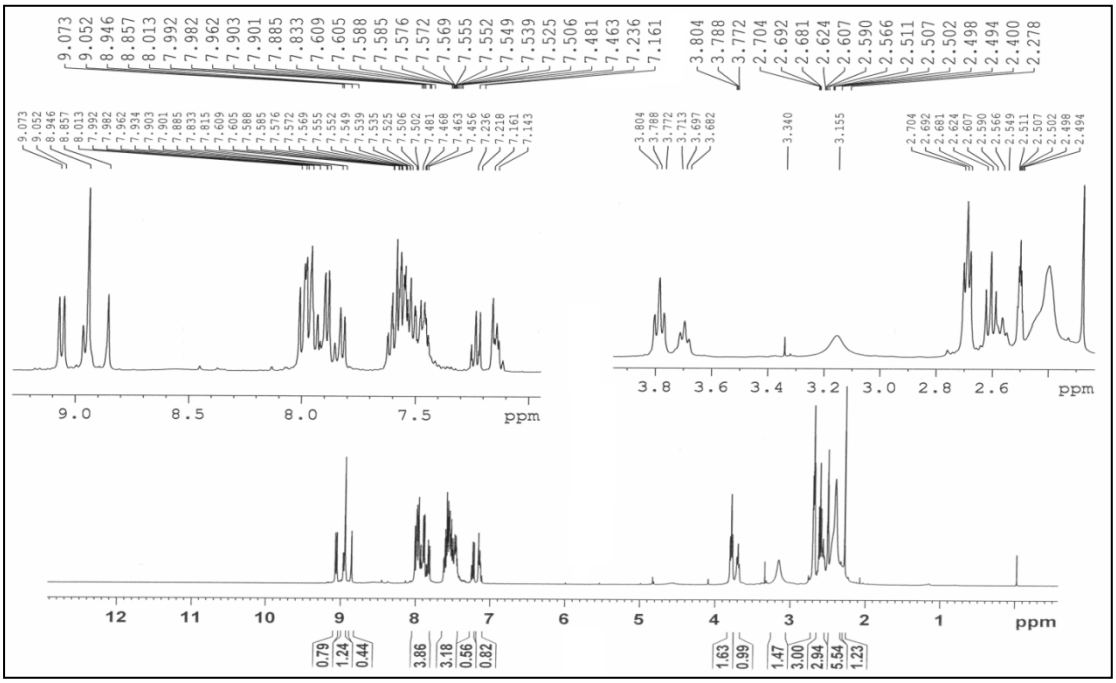

Figure S6. ^{1}H NMR spectrum of N-[Naphthyl methylidene]-2-piperazin-1-ylethanamine (L^2).

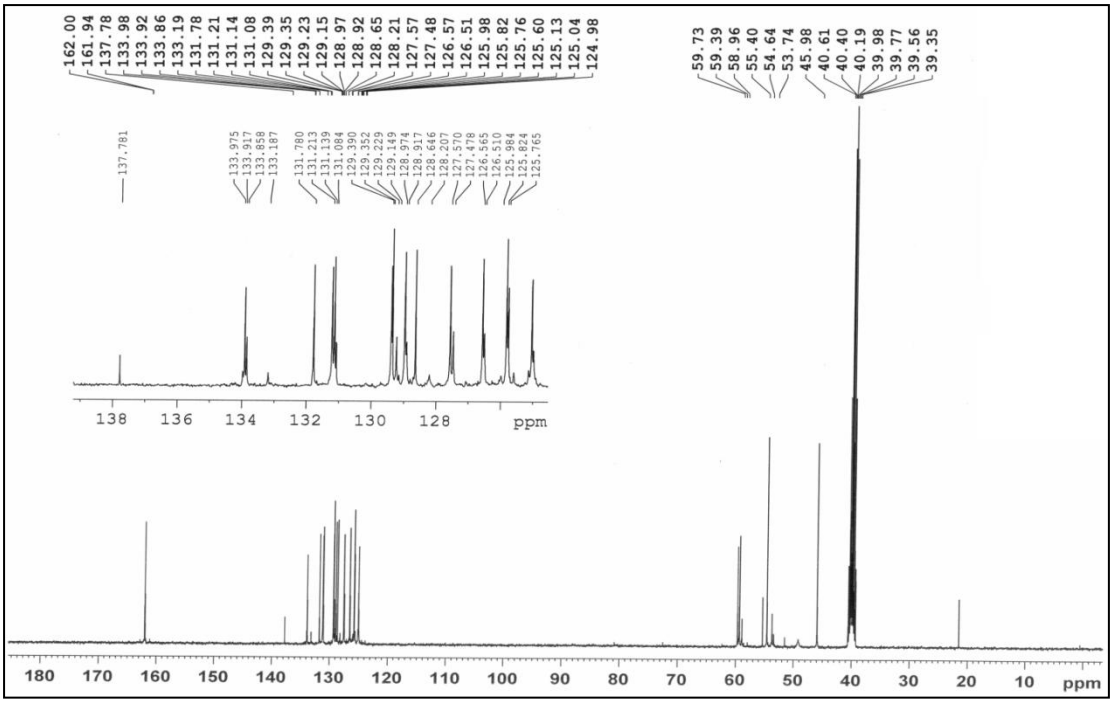

Figure S7. ^{13}C NMR spectrum of N-[Naphthyl methylidene]-2-piperazin-1-ylethanamine (L^2).

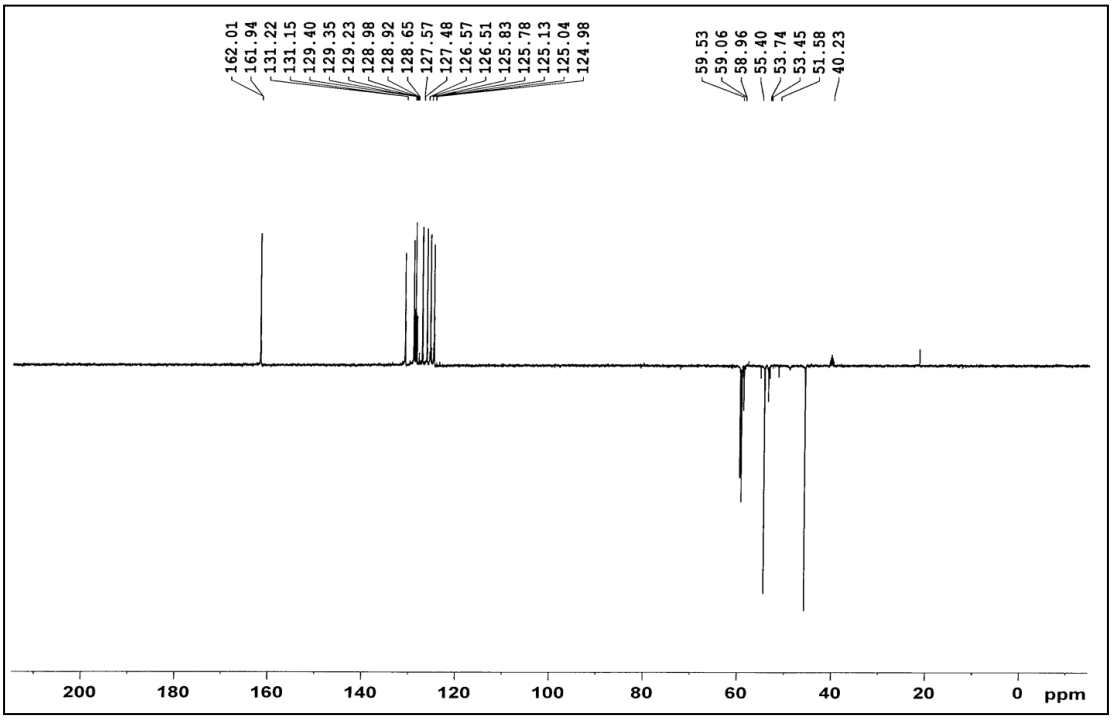

Figure S8. ^{13}C DEPT 135 NMR spectrum of N-[Naphthyl methylidene]-2-piperazin-1-ylethanamine (L^2).

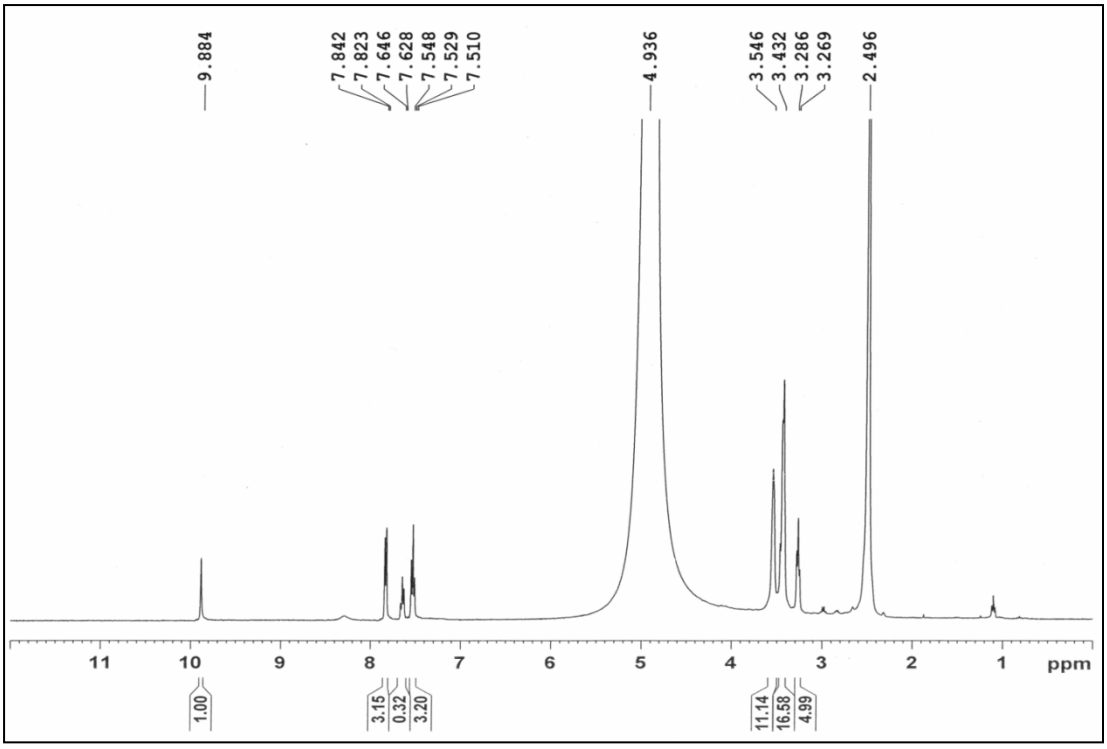

Figure S9. ^{1}H NMR spectrum of compound 2.

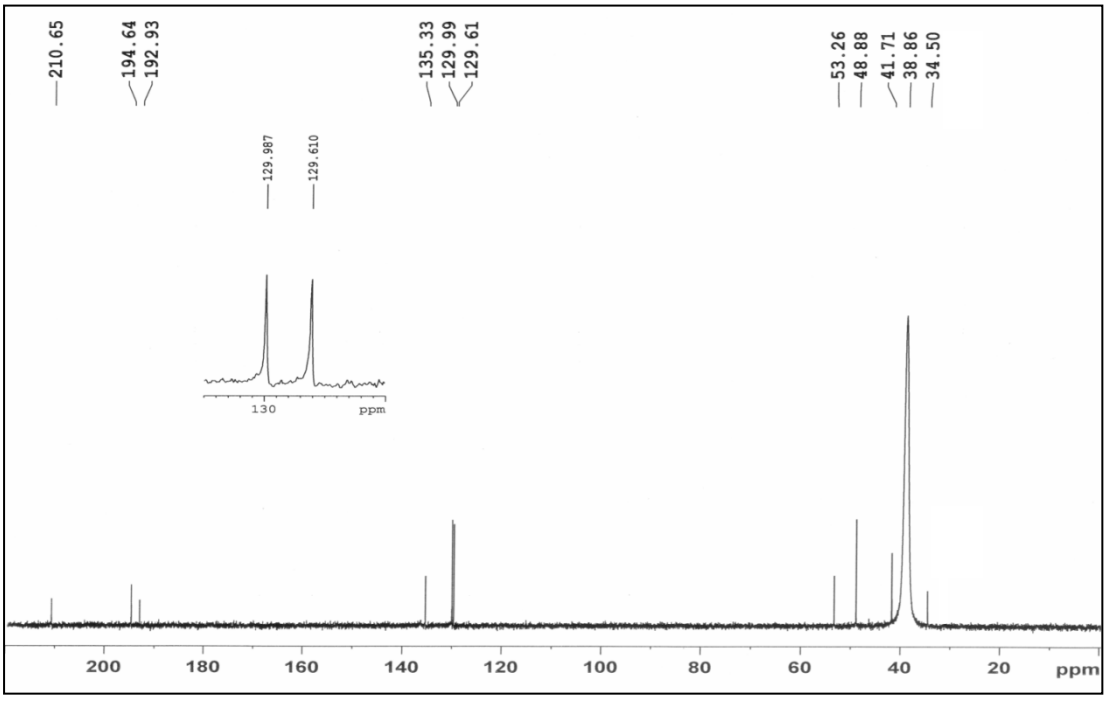

Figure S10. ^{13}C NMR spectrum of compound 2.

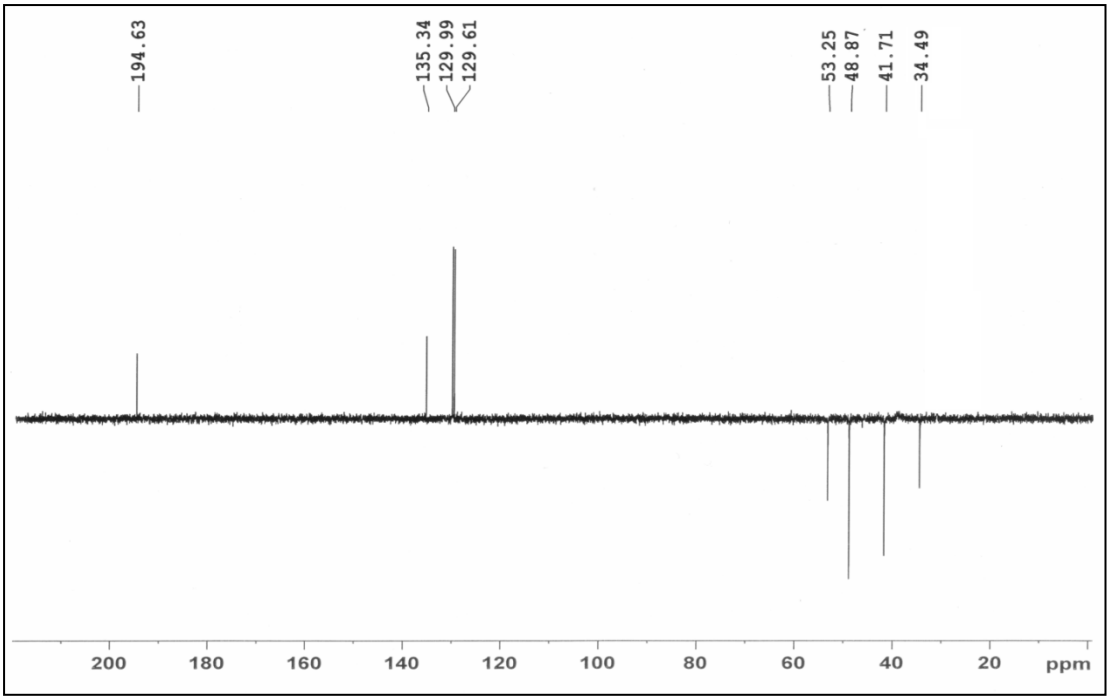

Figure S11. ^{13}C DEPT 135 NMR spectrum of compound 2.

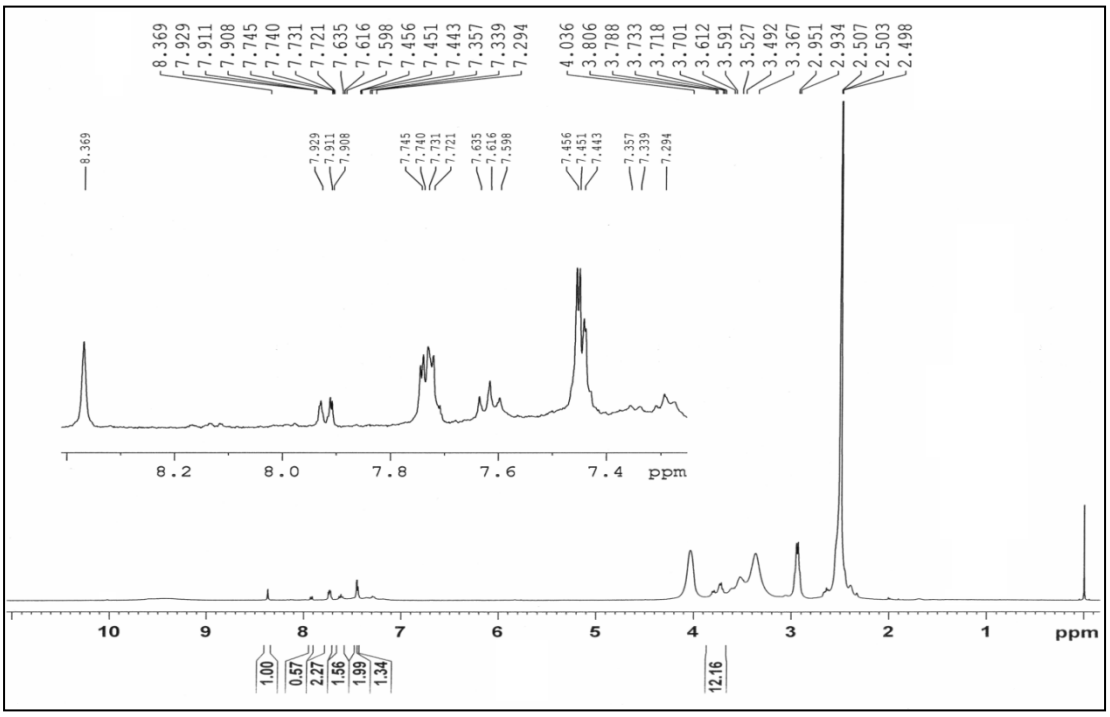

Figure S12. ^{1}H NMR spectrum of compound 4.

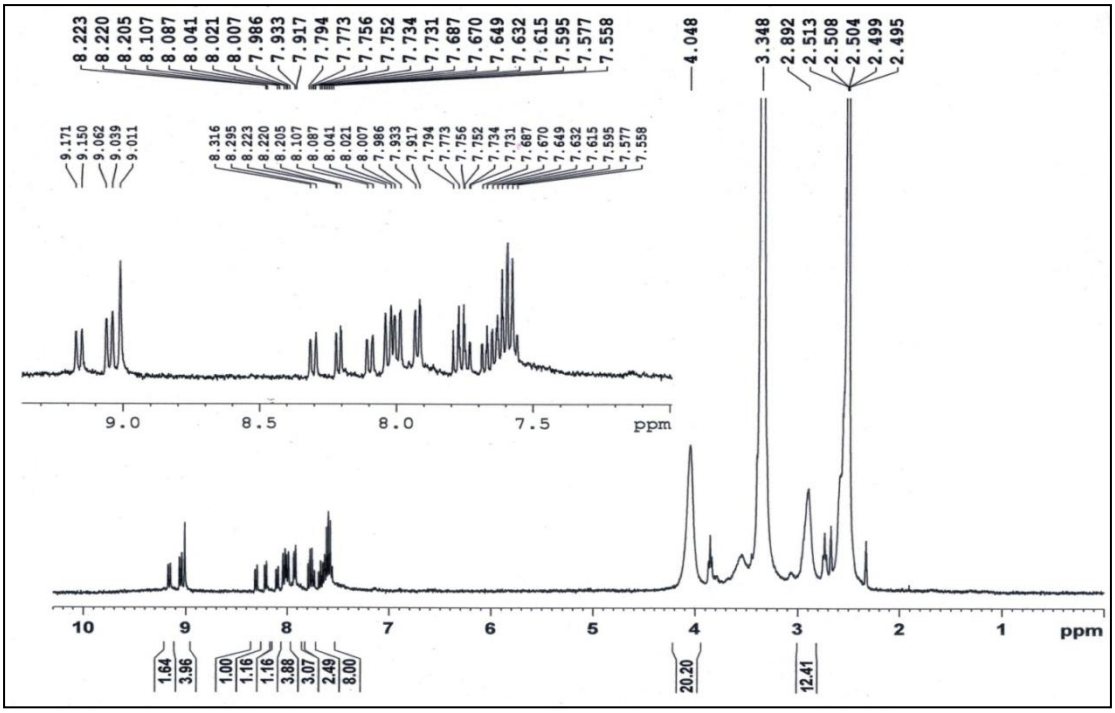

Figure S13. ^{1}H NMR spectrum of compound 8.

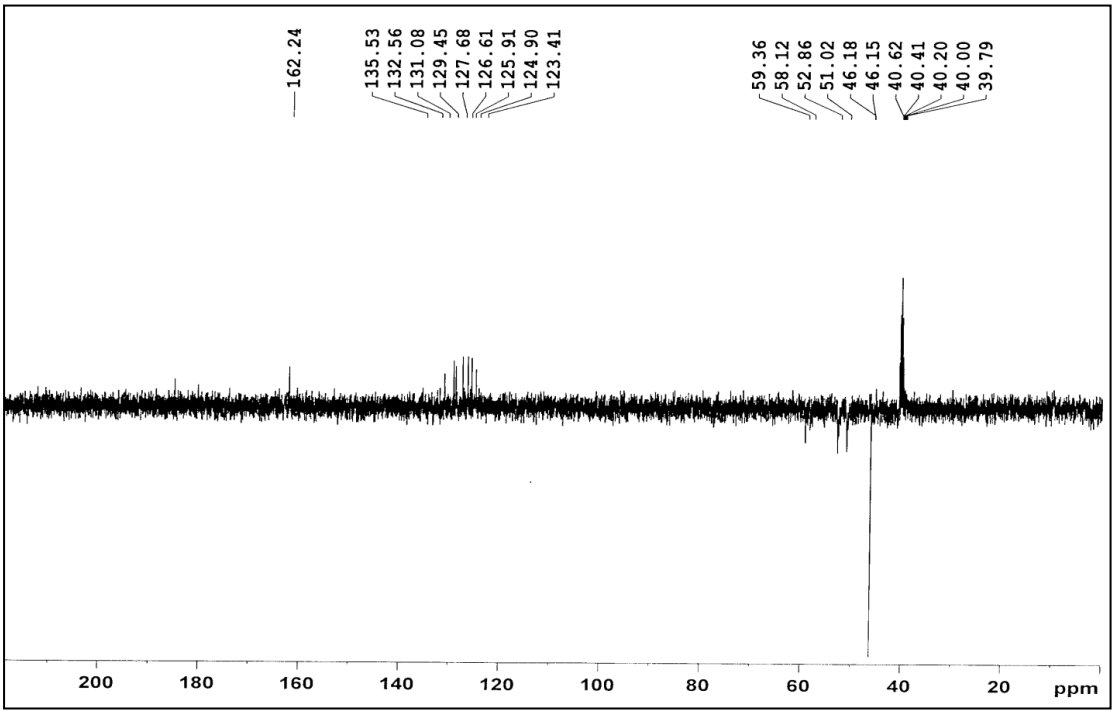

Figure S14. ^{13}C DEPT 135 NMR spectrum of compound 8.

3B.6.3. ESI MS spectra

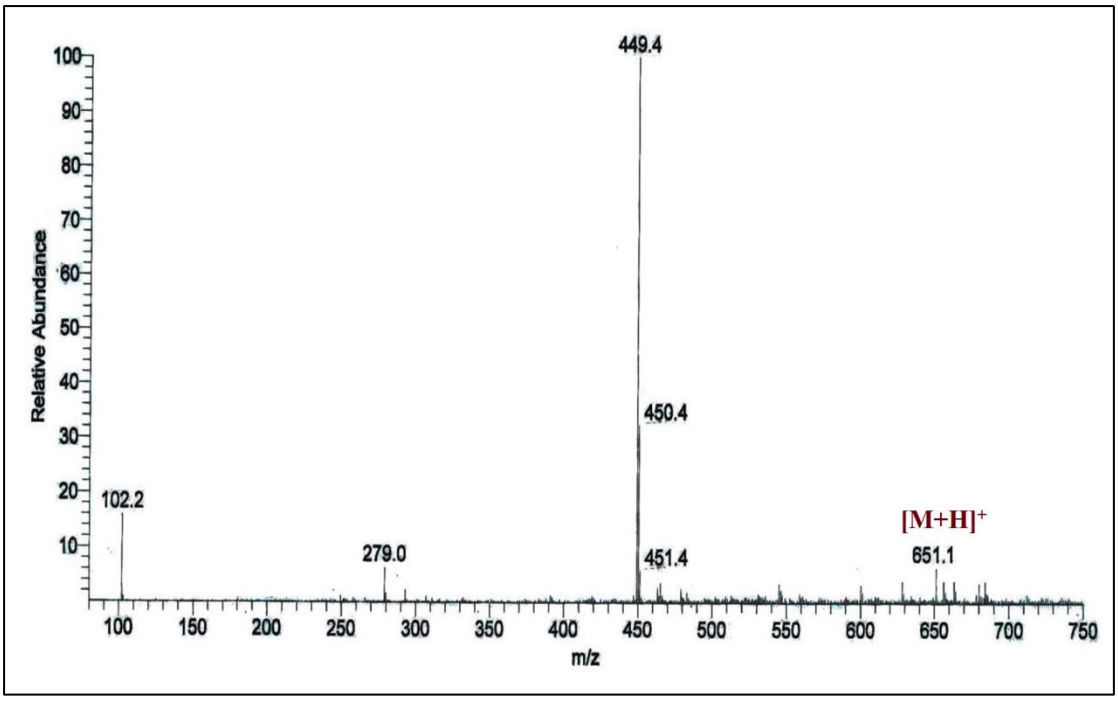

Figure S15. ESI MS spectra of compound 4.

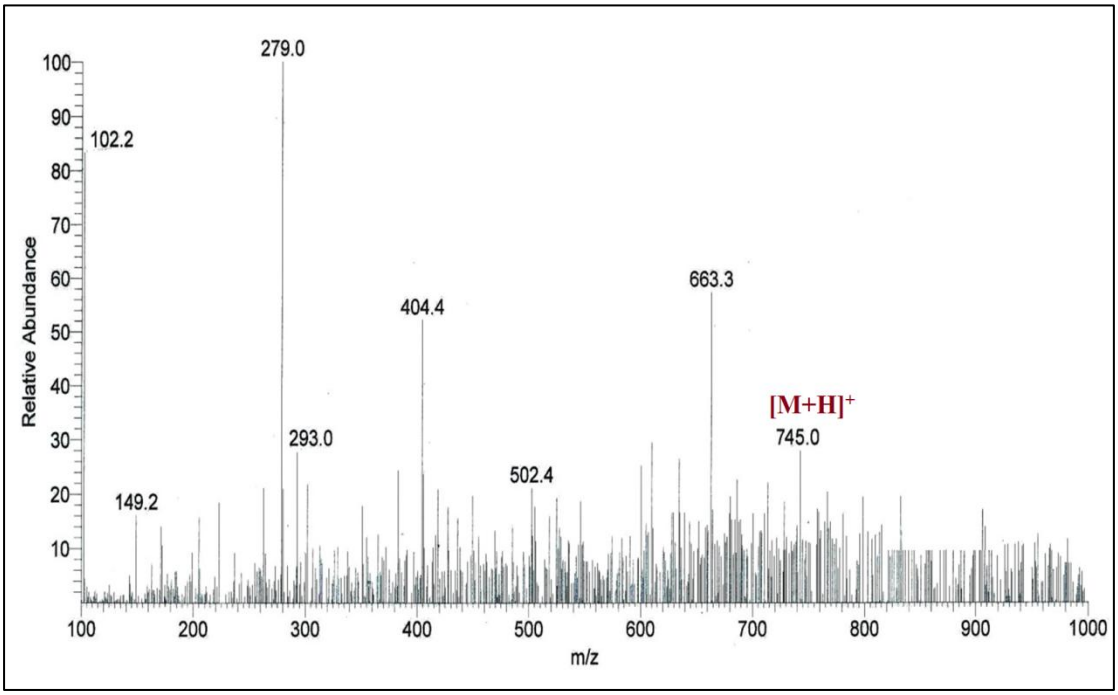

Figure S16. ESI MS spectra of compound 6.